J Geophys (1985) 58:27-43

Journal of Geophysics

Ray theory and its extensions: WKBJ and Maslov seismograms

C.H. Chapman

Department of Earth Sciences, University of Cambridge, Bullard Laboratories, Madingley Rise, Madingley Road, Cambridge CB3 OEZ, UK

Abstract. Asymptotic ray theory can be used to describe many seismic signals. Provided the wavefronts and amplitudes vary smoothly and the correct phase changes are included for caustics and reflection/transmission coefficients, it successfully describes direct and turning rays, on normal and reversed branches with multiple turning points, and partial and total reflections and transmissions. Nevertheless, many exceptions occur. Critical points, head waves, interference head waves, Airy caustics, Fresnel shadows, edge, point and interface diffractions and gradient coupling are examples discussed in this paper. Asymptotic ray theory can be simply extended to cover some of these problems. In this paper, the extension called the WKBJ or Maslov seismogram is discussed.

Key words: Geometrical and asymptotic ray theory – WKBJ and Maslov seismograms

Introduction

Seismic body waves can be described remarkably successfully using geometrical ray theory. Although much research on synthetic seismograms emphasizes situations in which geometrical ray theory breaks down, it should always be remembered that the majority of seismic data can be interpreted using geometrical ray theory. Most seismic body waves propagate with little dispersion or distortion, and non-geometrical effects are only important in limited regions. The classical Earth models of Jeffreys and Bullen, and Gutenberg were obtained using, for the most part, geometrical ray theory. Similarly, most seismic interpretation for oil exploration is based on geometrical ray theory. Nevertheless, non-geometrical affects are extremely important. By their very nature, interesting inhomogeneities in the Earth may cause non-geometrical signals. This paper will begin by reviewing asymptotic ray theory, the mathematical basis for geometrical ray theory. The various types of signals described by asymptotic ray theory in its basic form will be discussed. More importantly, the failures of geometrical ray theory will be emphasized: critical points, head waves, interference head waves, Airy caustics, Fresnel shadows, edge, point and interface diffractions, gradient coupling, etc. The numerical difficulties inherent in geometrical ray theory will also be discussed: the need for 'smooth' models in order to achieve meaningful geometrical amplitudes and efficient two-point ray tracing. No one method, except a purely numerical method such as finite differences, will solve all the problems mentioned above. Specialized canonical solutions are known for each problem separately. A major aim of theoretical seismologists is to obtain a simple, general method that will remain valid for the majority of realistic situations. In this paper, the generalization of asymptotic ray theory from the spatial domain to a phase space of position and slowness will be discussed. With this extension, ray theory remains valid at Airy caustics, Fresnel shadows, and critical points and head waves on plane interfaces. In its present form, problems with curved and discontinuous interfaces still remain. This inadequacy is to be expected as the boundary conditions, that are crucial for these signals, are only modelled locally. Similar limitations are to be expected for all extensions of ray theory that do not include appropriate boundary conditions.

Transforming the wave equation with respect to spatial coordinates, either 'globally', if the model is translationally invariant with respect to the coordinate or 'locally' otherwise, we obtain a new wave equation in slowness coordinates. Solutions of this wave equation can be obtained using asymptotic ray theory. The phase of this solution in slowness space is related to the spatial solution by the Legendre transformation. The nature of this transformation will be discussed in detail for various types of signal as it is crucial to the computation of synthetic seismograms. The amplitude function is obtained by canonical transformation.

Synthetic seismograms in the real spatial domain are obtained from the slowness domain via the Radon transform. Since the solution in the slowness domain is described by asymptotic ray theory, i.e. non-dispersive propagation, the Radon transform can be evaluated analytically. Synthetic seismograms calculated in this manner have been called 'WKBJ seismograms' in laterally homogeneous media and 'Maslov seismograms' in inhomogeneous media. Results for synthetic seismograms with various types of geometrical and non-geometrical signals will be described. Particular emphasis will be placed on the canonical problems mentioned above.

Although the theoretical methods for computing

synthetic seismograms may remain valid at high frequencies, and in general the accuracy may improve, in practice it is necessary to band-limit numerical results. Equivalently, we can smooth in the time domain. In order to obtain stable numerical results, this smoothing is essential and must be performed as an intrinsic part of the theory and not merely to the final numerical results. The smoothing can be achieved in various ways: including attenuation in the model, simply band-limiting the theory, or introducing a finite beam width into ray theory. The smoothing serves the additional purpose of reducing the sensitivity of calculations to small numerical features of the model. Therefore, the model need not be 'smooth' (as required by geometrical ray theory) and simpler interpolation methods can be used. A straightforward modelling method with linear velocity functions in triangles will be described. Analytic results for ray tracing and canonical transformations are known without the general difficulties of dynamic ray tracing. The overall result is an efficient, simple extension of geometrical ray theory that remains valid for some of the problem signals.

Geometrical ray theory (GRT)

First we will review the mathematical basis for GRT, usually called asymptotic ray theory (ART). ART (known by various names including "Debye series method" and "ray series method") has been widely discussed in the literature and several textbooks exist (Kline and Kay, 1965; Červený and Ravindra, 1971; Červený et al., 1977), the last two dealing specifically with the seismic or elastodynamic problem. The technique has been used to compute seismograms in inhomogeneous media (e.g. Hron and Kanasewich, 1971; Jackson, 1971; McMechan and Mooney, 1980; SEIS81 program, etc.). For simplicity, we present an outline of the theory for the scalar wave equation. More details, particularly the extension to elastodynamics, can be found in the above references.

Consider the simplest, scalar wave equation

$$\nabla^2 \phi - v^{-2}(\mathbf{x})\, \partial_t^2 \phi = 0. \tag{1}$$

It is notationally simpler in most expressions to use the wave slowness, $u(\mathbf{x})$, rather than the wave velocity, $v(\mathbf{x}) = u^{-1}(\mathbf{x})$. As is well known, in a homogeneous medium, solutions of the wave equation are non-dispersive, e.g.

$\phi(t, \mathbf{x}) = \phi_0(t - uR)$ for a plane wave

or

$\phi(t, \mathbf{x}) = \phi_0(t - uR)/R$ for a spherical wave.

The pulse shape remains constant, i.e. $\phi_0(t)$, and propagates with a constant velocity, v. The amplitude varies as geometrical spreading occurs. We therefore look for a similar solution in inhomogeneous media – a pulse propagating with the local velocity, $v(\mathbf{x})$, without distortion.

It is often convenient to work in the frequency domain. We take the Fourier transform (FT) of Eq. (1) with respect to time:

$$\hat{\phi}(\omega, \mathbf{x}) = \int_{-\infty}^{\infty} \phi(t, \mathbf{x})\, e^{i\omega t}\, dt$$
$$\phi(t, \mathbf{x}) = \frac{1}{2\pi} \int_B \hat{\phi}(\omega, \mathbf{x})\, e^{-i\omega t}\, d\omega. \tag{2}$$

We shall use the fact that the field variable, ϕ, is real [therefore, $\hat{\phi}(-\omega, \mathbf{x}) = \hat{\phi}^*(\omega, \mathbf{x})$] and causal (therefore, the Bromwich contour 'B' runs above any singularities in the complex ω-plane). With this transform, Eq. (2), and the usual conditions about the variable decaying as $t \to \infty$, we obtain the transformed wave equation

$$\nabla^2 \hat{\phi} + \omega^2 u^2(\mathbf{x})\, \hat{\phi} = 0. \tag{3}$$

In order to find a solution of this equation, we take as a trial solution

$$\hat{\phi}(\omega, \mathbf{x}) = \hat{\phi}_0(\omega) \sum_{n=0}^{\infty} \frac{A^{(n)}(\mathbf{x})}{(-i\omega)^n}\, e^{i\omega T(\mathbf{x})}, \tag{4}$$

The important features of this ansatz are the separation of frequency, ω, and spatial $\mathbf{x}$, dependence and the linear frequency dependence of the phase. At high frequencies, only the leading term will be important and we have a pulse, $\phi_0(t)$, propagating without distortion and with propagation time, $T(\mathbf{x})$ and an amplitude variation $A^{(0)}(\mathbf{x})$, i.e. $\phi(t, \mathbf{x}) = A^{(0)}(\mathbf{x})\, \phi_0[t - T(\mathbf{x})]$. At finite frequencies, the high-order terms allow for distortion of the pulse as the amplitude coefficients, $A^{(n)}(\mathbf{x})$, differ.

In the time domain, the series (4) reduces to

$$\phi(t, \mathbf{x}) = \mathrm{Re}\left\{ \Phi_0(t) * \sum_{n=0}^{\infty} A_+^{(n)}(\mathbf{x})\, h^{(n)}[t - T(\mathbf{x})] \right\} \tag{5}$$

where we have anticipated some of the generalities we will require later by permitting complex amplitude coefficients, $A^{(n)}(\mathbf{x})$. The discontinuity functions, $h^{(n)}(t)$, are

$$h^{(0)}(t) = \delta(t), \quad h^{(1)}(t) = H(t), \quad h^{(2)}(t) = t\, H(t), \ \ldots$$

i.e. the Dirac delta function, Heaviside step function, and higher-order integrals. Convolved with the pulse, $\phi_0(t)$ (the convolution operator is represented by the star (*) in the usual fashion), they cause n-th order integration. Higher-order terms are therefore smoother than lower-order terms. The function, $\Phi_0(t)$, represents the analytic time series corresponding to the real series, $\phi_0(t)$, i.e.

$$\Phi_0(t) = \phi_0(t) + i\, \bar{\phi}_0(t) \tag{6}$$

where $\bar{\phi}_0(t)$ is the Hilbert transform of $\phi_0(t)$. The spectra are related via $\hat{\bar{\phi}}_0(\omega) = -i\, \mathrm{sgn}(\omega)\, \hat{\phi}_0(\omega)$ and $\hat{\Phi}_0(\omega) = 2H(\omega)\, \hat{\phi}_0(\omega)$. Although we have assumed the amplitude coefficients are independent of frequency, Eq. (4), they must be conjugate for positive and negative frequencies in order to obtain a real solution, i.e.

$$A_+^{(n)}(\mathbf{x}) = A_-^{(n)*}(\mathbf{x})$$

where the subscript $(\pm)$ indicates whether $\omega \gtrless 0$. In expression (5), the sign for positive frequencies should be used.

In the wave equation, Eq. (1), and the solution, Eq. (5), we have not explicitly mentioned the source. More properly, Eq. (1) should contain an inhomogeneous source term, and amplitudes and travel time in Eq. (5) should refer to this source. For simplicity, we omit these details.

Without going into mathematical detail, it is evident from the time form of Eq. (5) that the series is asymptotic. At sufficiently large time, the highest-order term included in the series dominates, $O(t^{n-1})$, and diverges. This cannot occur if the series converged to the exact solution.

Finally, we should note that although we have only included one series in Eq. (4), often multiple solutions for $T(\mathbf{x})$ and $A^{(n)}(\mathbf{x})$ exist. Then a summation over these different rays is implied.

Substituting the ansatz (4) in the wave equation (3), we obtain a series in inverse powers of frequency. Setting the coefficient of each power of ω equal to zero, we obtain the eikonal equation

$$(\nabla T)^2 - u^2(\mathbf{x}) = 0 \tag{7}$$

and the general transport equation

$$2\nabla T \cdot \nabla A^{(k+1)} + A^{(k+1)} \nabla^2 T + \nabla^2 A^{(k)} = 0. \tag{8}$$

The solution of the eikonal equation (7), defines the function, $T(\mathbf{x})$. We call constant surfaces, $t = T(\mathbf{x})$, wavefronts and define the slowness vector

$$\mathbf{p} = \nabla T \tag{9}$$

perpendicular to these surfaces (Fig. 1). Rays propagate in the direction $\mathbf{p}$, so if $\mathbf{x}$ defines the ray position

$$\mathbf{p} = u \frac{d\mathbf{x}}{ds} = \dot{\mathbf{x}} \tag{10}$$

where $d\mathbf{x}/ds$ is a unit vector (s is the arc length along the ray) and $|\mathbf{p}| = u$ from the eikonal equation [Eqs. (7) and (9)]. The superscript dot ($\dot{}$) represents d_v where the differential is related to the arc length and travel time by $dv = v\,ds = v^2\,dT$. Differentiating Eq. (9), we obtain

$$\dot{\mathbf{p}} = u \frac{d}{ds}(\nabla T) = u \nabla \left(\frac{dT}{ds}\right) = u \nabla u \tag{11}$$

as $dT/ds = u$ from Eq. (7). These equations, Eqs. (10) and (11), can be written in the form of Hamilton's equations (Kline and Kay, 1965, Chap. 3). If we define a Hamiltonian

$$H(\mathbf{x}, \mathbf{p}) = \tfrac{1}{2}[\mathbf{p}^2 - u^2(\mathbf{x})], \tag{12}$$

the eikonal equation (7) is equivalent to $H = 0$ [with Eq. (9)]. This can be solved by the method of characteristics (Courant and Hilbert, 1962, Vol. II, Chap. 2). The Hamilton or bicharacteristic equations are

$$\begin{aligned} \dot{\mathbf{x}} &= \nabla_{\mathbf{p}} H = \mathbf{p} \\ \dot{\mathbf{p}} &= -\nabla_{\mathbf{x}} H = u \nabla u \end{aligned} \tag{13}$$

the same as Eqs. (10) and (11). Compared with mechanics, slowness and the differential dv have replaced velocity and the differential dT. The Lagrangian of the system is derived from the Hamiltonian (12) by means of the Legendre transformation (Kline and Kay, 1965, p. 116):

$$\begin{aligned} L(\mathbf{x}, \dot{\mathbf{x}}) &= \mathbf{p} \cdot \dot{\mathbf{x}} - H(\mathbf{x}, \mathbf{p}) \\ &= u(\mathbf{x}) |\dot{\mathbf{x}}|. \end{aligned} \tag{14}$$

The Lagrangian satisfies the Euler-Lagrange equations and so the travel-time integral along the ray path is stationary (Fermat's or Hamilton's principle), and is given by

$$\begin{aligned} T(\mathbf{x}) &= \int_v^v L(\mathbf{x}, \dot{\mathbf{x}})\, dv = \int_s^s u\, ds \\ &= \int_v^v (L + H)\, dv = \int_{\mathbf{x}}^{\mathbf{x}} \mathbf{p} \cdot d\mathbf{x}. \end{aligned} \tag{15}$$

In order to find the amplitude coefficient $A^{(0)}$, we solve the first transport equation (8) with $k = -1$. Using the definition (9), it can be rewritten

$$d_v \ln A^{(0)} = -\nabla \cdot \mathbf{p} \tag{16}$$

where we have used the identity $\mathbf{p} \cdot \nabla \equiv d_v$. We use Smirnov's lemma (Smirnov, 1964, p. 442) to solve this equation. Other more physical proofs have been given in the references quoted above. Consider the Jacobian

$$D = \left. \frac{\partial \mathbf{x}}{\partial \mathbf{x}_0} \right|_v \tag{17}$$

where $\mathbf{x}_0$ is an initial point on a ray and $\mathbf{x}$ defines a ray path. Expanding the derivative of D, the determinants contain elements such as $\partial \dot{x}_i / \partial x_{0j} = \partial p_i / \partial x_{0j}$ [using Eq. (10)]. Expanding these partial derivatives, $\partial p_i / \partial x_{0j} = (\partial p_i / \partial x_k)(\partial x_k / \partial x_{0j})$, most terms do not contribute (as rows of the determinants are linearly dependent) and only the terms $(\partial p_i / \partial x_i)(\partial x_i / \partial x_{0j})$ (no summation) are important. Thus

$$\dot{D} = (\nabla \cdot \mathbf{p}) D. \tag{18}$$

Combining Eqs. (16) and (18), we have

$$d_v \ln (A^{(0)2} D) = 0$$

and

$$A^{(0)}(\mathbf{x}) = A^{(0)}(\mathbf{x}_0) \left(\left. \frac{\partial \mathbf{x}}{\partial \mathbf{x}_0} \right|_v \right)^{-\frac{1}{2}}. \tag{19}$$

We can relate the Jacobian to the cross-sectional area of a ray tube (Fig. 2). It is important to note that in defining the Jacobian (17), the independent variable is v, not the more usual T. The volume elements illustrated in Fig. 2 which are related by the Jacobian D are defined by cross-sections J and J_0 and lengths $ds = u\,dv$ and $ds_0 = u_0\,dv$. Hence

$$D = J\,ds / J_0\,ds_0.$$

The result that the amplitude is proportional to $(uJ)^{-\frac{1}{2}}$ is equivalent to conservation of energy as it propagates along the ray tube.

In order to compute the partial derivatives required for the Jacobian (17), it is necessary to solve the neighbouring ray equations (otherwise known as the paraxial

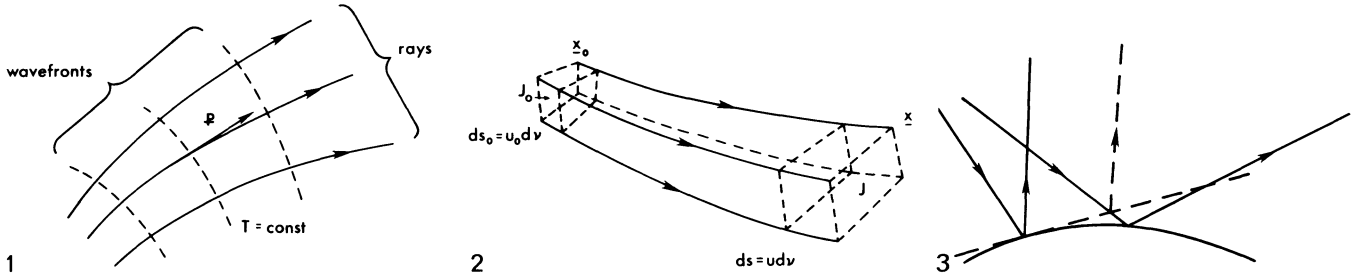

Fig. 1. Rays and wavefronts: wavefronts are defined by the equation $t = T(\mathbf{x})$, and rays are trajectories perpendicular to these surfaces

Fig. 2. A ray tube with cross-sectional area J_0 at $\mathbf{x}_0$ spreading to area J at $\mathbf{x}$

Fig. 3. Rays reflecting from an interface according to Snell's law. Note the increase in spreading caused by the curvature of the interface

equations or dynamic ray tracing). Perturbing the ray equations (13) we obtain the differential system

$$\begin{aligned} \delta\dot{\mathbf{x}} &= \delta\mathbf{p} \\ \delta\dot{\mathbf{p}} &= \mathbf{C}\,\delta\mathbf{x} \end{aligned} \tag{20}$$

where $\mathbf{C}$ is the symmetric 3×3 matrix

$$C_{ij} = \frac{\partial u}{\partial x_i}\frac{\partial u}{\partial x_j} + u\frac{\partial^2 u}{\partial x_i \partial x_j}.$$

Solving the sixth-order system with appropriate initial conditions, the required partial derivatives can be obtained. We will not dwell here on the alternative forms of Eq. (20) that have been derived, nor the difficulties caused by the singularities at caustics. In this paper we will only need analytic solutions known for simple models (see section on 'A numerical model' below).

An important property of the differential system (20) is that the trace of the differential matrix is zero. As a consequence, the determinant of the propagator matrix is unity (the Jacobi identity, Gilbert and Backus (1966)]. Liouville's theorem results

$$\left.\frac{\partial(\mathbf{x}, \mathbf{p})}{\partial(\mathbf{x}_0, \mathbf{p}_0)}\right|_v = 1. \tag{21}$$

The differential system and the propagator matrix also have symplectic symmetries. Important properties of beams follow but this need not concern us here. More details concerning the Hamilton equations and Liouville's theorem can be found in Thomson and Chapman (1985).

We have seen that the mathematical structure of GRT is straightforward and fundamental. The *kinematic ray equations* (13) have the form of *Hamilton's equations*. The *Lagrangian* (14) is related to the *Hamiltonian* (12) by the *Legendre transformation*, and the travel time given by its line integral (15). The amplitude coefficient can be found by a *canonical transformation* (19) and the *Jacobian* derived from the *dynamic ray equations* (20).

In the next section we briefly review differences that occur for elastic waves in media with interfaces and in the following section describe situations in which GRT is valid or invalid.

Elastic waves and interfaces

The wave equations for elastic waves are significantly more complicated than for scalar waves, Eq. (1), not least because we are concerned with a vector equation. Nevertheless, the same basic technique can be used to look for an asymptotic solution. Substituting an asymptotic series in inverse powers of frequency into the wave equations, eikonal and transport equations are obtained. Algebraic details can be found in Červený and Ravindra (1971). Two eikonal equations are obtained corresponding to the two wave types permitted. If the wave speed is the *P*-wave velocity, $v(\mathbf{x}) = \alpha(\mathbf{x})$, the displacement of the first amplitude coefficient must be longitudinal, and if the speed is the *S*-wave velocity, $v(\mathbf{x}) = \beta(\mathbf{x})$, the displacement transverse. The transport equations are more complicated, but the solution is remarkably similar. For *P* waves, the magnitude of the displacement is

$$A^{(0)}(\mathbf{x}) = A^{(0)}(\mathbf{x}_0)\left(\frac{\rho\alpha^2}{\rho_0\alpha_0^2}\left.\frac{\partial \mathbf{x}}{\partial \mathbf{x}_0}\right|_v\right)^{-\frac{1}{2}} \tag{22}$$

and the displacement is directed along the ray, i.e. in the direction $\mathbf{p}$. In general, the *S*-wave situation is more complicated as the polarization must be considered in the transport equation, but the magnitude is given by Eq. (22) with the *S*-wave velocity substituted. More details can be found in Červený and Ravindra (1971).

Implicitly it was assumed above that the medium was continuous. In fact, in order to find the n-th term in the asymptotic series, it is necessary that the n-th derivatives of the medium are continuous, i.e. the model contains no $(n+1)$-th or lower-order discontinuities. If the model contains $(n+1)$-th order discontinuities, the asymptotic series must be terminated at the $(n-1)$-th term, i.e. for second-order discontinuities (gradient discontinuities), the zeroth term is valid. For first-order discontinuities no terms are valid and we must match boundary conditions at the interface.

At an interface, reflected and transmitted rays of all types may be generated. In order to connect solutions of the kinematic ray equations, Snell's law is used, i.e. the component of the slowness vector parallel to the interface is conversed and the other components are modified to make the appropriate Hamiltonian zero. Necessarily, there will now be many solutions (rays)

and, in principle, it is necessary to continue all their ray series. For the dynamic tracing, account must also be taken of the interface curvature which will modify the spreading of a ray tube (Fig. 3). In addition, boundary conditions must be solved for the continuity of displacement and normal traction at the interface (assuming a welded solid/solid interface). These simple physical ideas lead to straightforward but tedious algebra. The results can be found in Červený and Ravindra (1971). For the zeroth amplitude coefficient, the reflection and transmission coefficients are identical to the coefficients for a plane wave at a plane interface. The amplitude coefficient for each ray type must be multiplied by the appropriate reflection and transmission coefficient. Care must be taken that the change in spreading caused by reflection or transmission even for a plane interface is not duplicated in the spreading and coefficient calculations. Also, the coefficient must be with respect to the appropriate wave property, e.g. displacement magnitude.

Canonical ray problems

In this section we describe, largely through diagrams, body waves for which ART is valid or invalid. In the latter case, we give references for techniques that have been used to solve the problem.

a) *Direct rays*

In Fig. 4a we illustrate the simplest type of rays spreading from a point source. The model contains no discontinuities and the ray paths and amplitude coefficients vary smoothly. This is a situation for which ART is an excellent approximation.

b) *Normal turning rays*

In Fig. 5a, the ray paths and amplitudes again vary smoothly and there appears to be little difference from Fig. 4a. Indeed the final results are similar. However, in Fig. 5a turning points exist (for which $\mathbf{p}$ and Vv are perpendicular). Mathematically, the difference is important because partial derivatives in the dynamic ray equations (20) have singularities. Again, ART is an excellent approximation.

c) *Reversed turning rays*

If the rays cross (Fig. 6a), then the amplitude coefficient is infinite and obviously ART breaks down. The singularity is called a caustic. Special methods are needed in the vicinity of the caustic (see g) below). Nevertheless, ART can still be used beyond the caustic provided the amplitude coefficient is interpreted correctly. At the simplest caustic, the Jacobian (17) changes sign. Equation (19) for the amplitude coefficient remains valid, provided the correct square root is used. We replace Eq. (19) by

$$A^{(0)}(\mathbf{x}) = A^{(0)}(\mathbf{x}_0) \left| \frac{\partial \mathbf{x}}{\partial \mathbf{x}_0} \right|_v^{-\frac{1}{2}} e^{i \operatorname{sgn}(\omega) \frac{\pi}{2} \sigma(\mathbf{x}, \mathbf{x}_0)} \tag{23}$$

where $\sigma(\mathbf{x}, \mathbf{x}_0)$ is the KMAH index [after the contributions by Keller (1958), Maslov (1965), Arnol'd (1967) and Hörmander (1971)]. The KMAH index, initially zero [$\sigma(\mathbf{x}_0, \mathbf{x}_0) = 0$], is constant between caustics on a ray and changes by an integer as each caustic is passed (Keller, 1958). For seismic body waves the KMAH index always increases (Červený and Ravindra, 1971, p. 76) as the phase and group velocities are in the same direction. The increment of the index at a caustic is the number of dimensions a ray tube loses at the caustic (Keller, 1958). Normally, the cross-section of a ray tube is reduced to a line and the KMAH index increases by unity. This introduces the familiar phase retardation of $\pi/2$. Alternatively, the ray tube may be reduced to a point and two dimensions are lost. Then the phase shift is π. The origin of the $\pi/2$ phase shift can be investigated using the canonical Airy caustic problem (see g) below) (Ludwig, 1966).

d) *Reflected and transmitted rays*

Provided an interface is smooth and the reflection/transmission coefficient only varies slowly, then ART can be used (Fig. 7a). The geometrical spreading is modified by the curvature of the interface and the amplitude by the reflection/transmission coefficient. For total reflections, the coefficient is complex but expression (5) remains valid. ART breaks down if the shape of the interface or the behaviour of the coefficients cause discontinuous (or rapid) amplitude variations across the wavefronts. Examples are the critical point (see e) below) or corner diffractions (see i) below).

The rays already illustrated can be described by ART. We now come on to the many types of body waves for which ART, in its simplest form, breaks down. Many of these signals are very important, as they can be used to investigate inhomogeneities in the Earth.

e) *Critical rays and head waves*

At the critical angle, the reflection coefficient has a square root singularity. The grazing transmitted ray has zero geometrical amplitude. The discontinuity in the reflected wavefront and the transmitted wavefront are connected by another wavefront, the head wave (Fig. 8a). Simple ART does not describe the head wave or the critical region. The head wave can be described by the first-order term, $A^{(1)}(\mathbf{x})$, in ART (Červený and Ravindra, 1971). A more complicated function (the Weber function) is needed to describe the solution in the neighbourhood of the critical point (Marks and Hron, 1977).

f) *Interference head wave*

In practice, a simple head wave rarely exists. Invariably a velocity gradient below the interface causes a turning ray with a very similar travel time (Fig. 9a). Multiple turning rays reflecting below the interface will also exist. The normal head wave is the limiting case. Although each ray path can be described by ray theory, ART will be of limited validity due to the proximity of the interface to the ray path. More accurate wave functions (the Airy function) are required in the faster medium (Hill, 1973; Červený and Ravindra, 1971, Chap. 6).

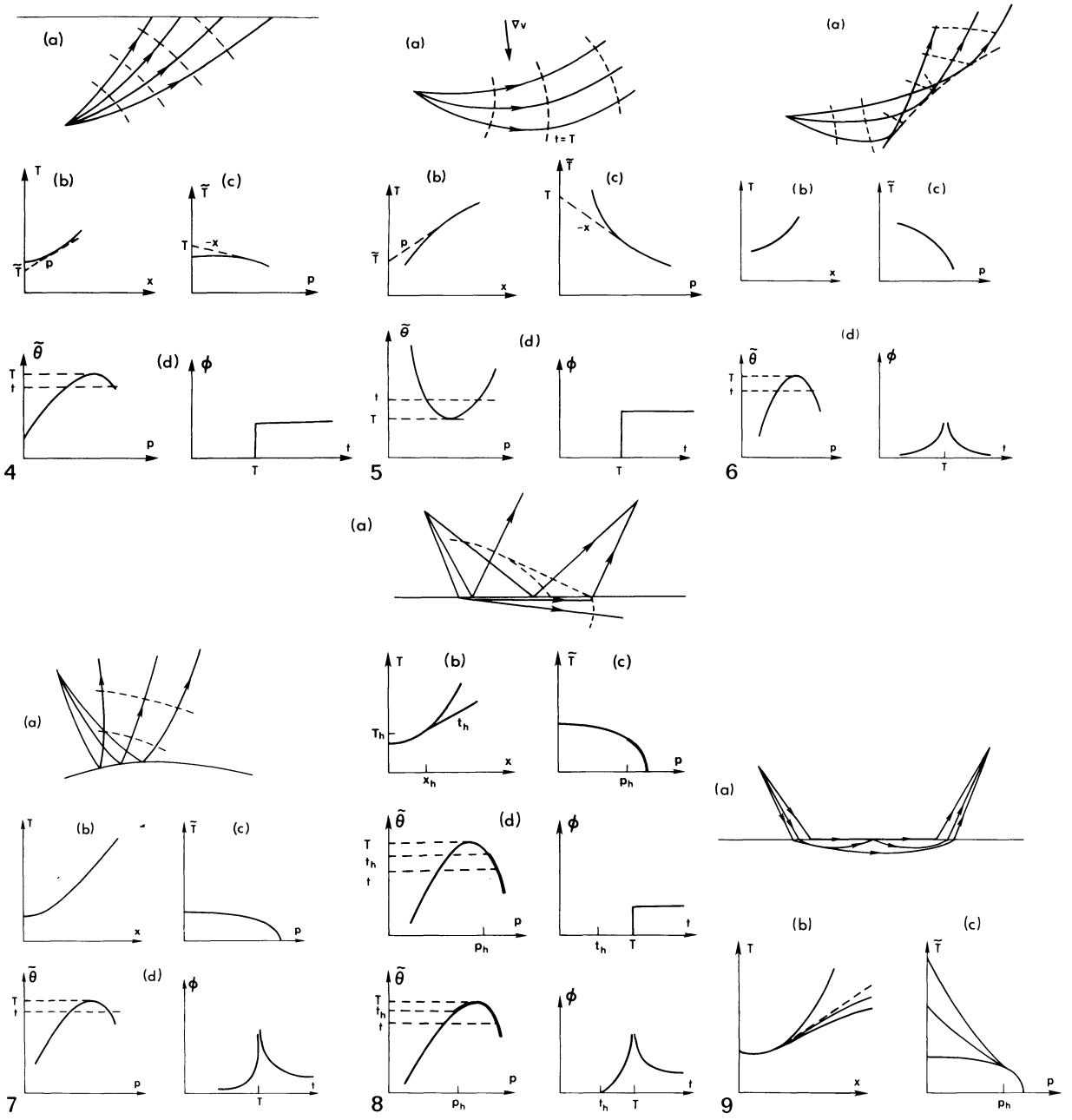

Fig. 4a–d. Diagrams for direct rays: **a** typical ray paths and wavefronts; **b** the travel-time curve, $T(x)$; **c** the intercept time $\tilde{T}(p)$; **d** the function, $\tilde{\theta}(p, \mathbf{x})$, and a typical seismogram if $\phi_0(t) = H(t)$

Fig. 5a–d. As Fig. 4, but for normal turning rays

Fig. 6a–d. As Fig. 4, but for reversed turning rays

Fig. 7a–d. As Fig. 4, but for a reflection. The seismogram is illustrated for a total reflection

Fig. 8a–d. As Fig. 4, but for a head wave and critical point. In **d**, the function, $\tilde{\theta}(p, \mathbf{x})$, and seismograms are illustrated for two cases: the receiver is either before (*top*) or after (*bottom*) the critical point

Fig. 9a–c. Diagrams for an interference head wave with only one multiple refraction shown: **a** typical ray paths; **b** the travel-time curves, $T(x)$; **c** the intercept times, $\tilde{T}(p)$

g) *Airy caustics*

At a caustic, ART breaks down as the geometrical amplitude is infinite. Near the caustic, the amplitude varies rapidly and the two rays interfere (Fig. 10a). Using higher-order terms in ART does not improve this situation. Rather, a more complicated ansatz must be used (Ludwig, 1966) which includes the expected behaviour near caustics (the Airy function in the frequency domain).

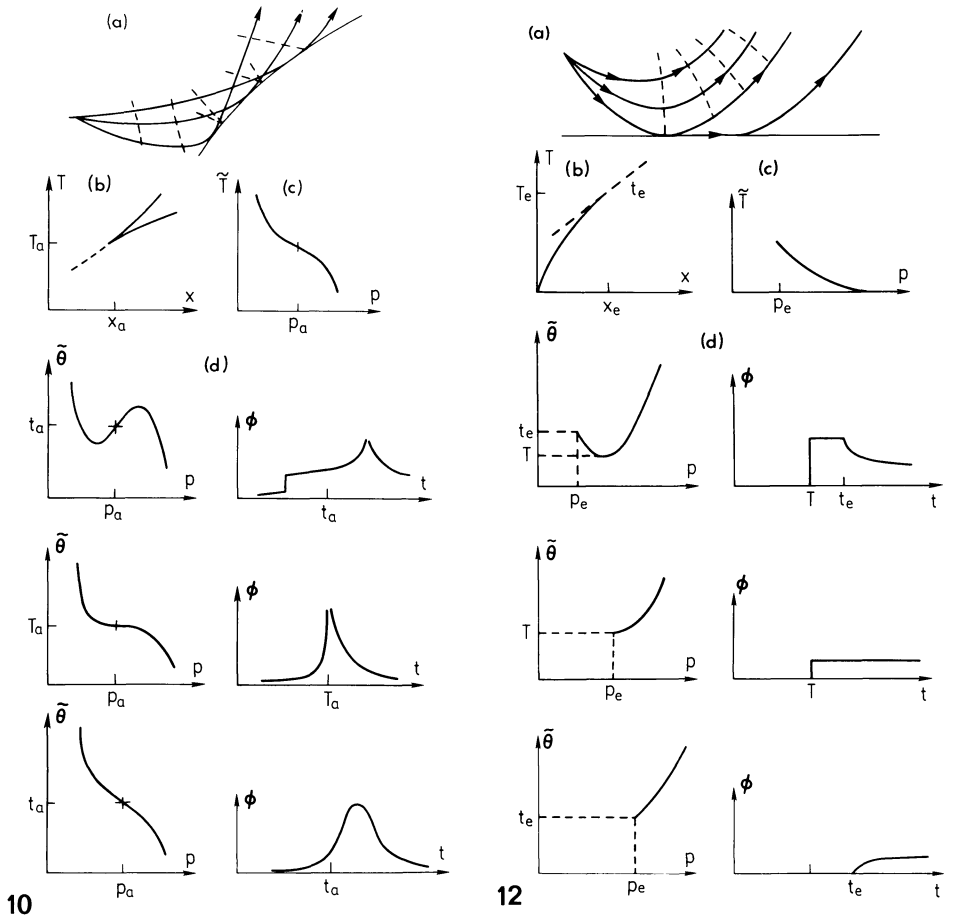

Fig. 10 a–d. As Fig. 4, but for an Airy caustic. In **d**, the function, $\tilde{\theta}(p, \mathbf{x})$, and seismograms are illustrated for three cases: the receiver is either in the illuminated region (*top*), at the caustic (*middle*) or in the shadow (*bottom*)

Fig. 12 a–d. As Fig. 4, but for a shadow. The wavefronts are discontinuous at the grazing ray. The resultant Fresnel diffraction is illustrated. In **d**, the function, $\tilde{\theta}(p, \mathbf{x})$, and seismograms are illustrated for three cases: the receiver is either in the illuminated region (*top*), at the shadow edge (*middle*) or in the shadow (*bottom*). In addition, an interface diffraction is generated

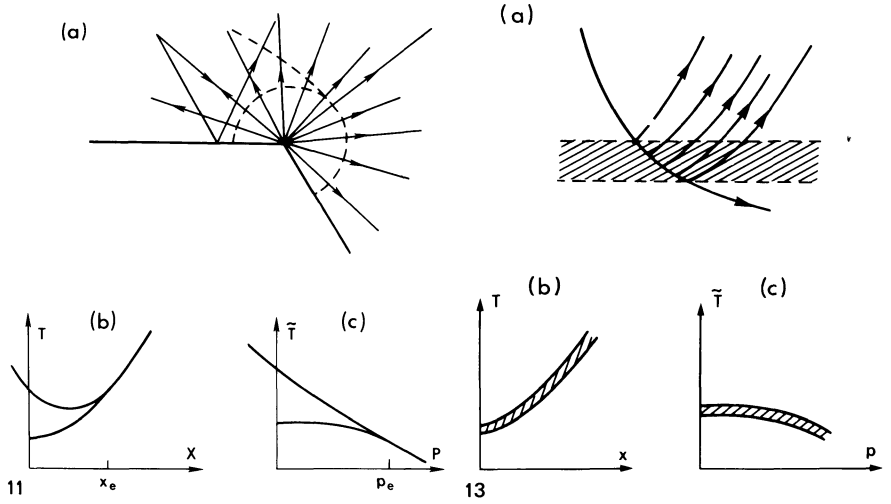

Fig. 11 a–c. As Fig. 9, but for an interface discontinuity. The reflected wavefront is discontinuous at the shadow edge, and edge or point diffractions are generated by the corner

Fig. 13 a–c. As Fig. 9, for a 'reflected' signal due to gradient coupling

h) *Fresnel shadows*

Various features in the model may cause the wavefronts to be discontinuous, e.g. reflections from a discontinuous interface (Fig. 11a) or rays grazing an interface (Fig. 12a). Although the geometrical amplitude is finite, ART is inaccurate. Two effects are important: the interface may generate new waves and non-geometrical effects occur at the shadow edge. The former requires the correct boundary conditions to be modelled, normally via a canonical problem. The latter is more straightforward as the wave function in the frequency domain is described by the Fresnel function.

i) *Edge and point diffractions*

If an interface is discontinuous, diffracted signals are generated at the corner (Fig. 11a). Keller (1962) has developed an extension of ART, geometrical diffraction theory, that can be used for these signals. ART is used to describe the wave incident on the corner and generated by the corner, and a canonical local problem is used to connect these rays by a direction-dependent diffraction coefficient which is a simple function of frequency.

j) *Interface diffractions*

If a ray grazes an interface (Fig. 12a), an interface wave is generated. The decay in the shadow is described by this wave. It is necessary to solve boundary conditions for a grazing ray and an interface. The amplitude and velocity of the signal are frequency dependent. Solutions have been given by Gilbert (1960) and Knopoff and Gilbert (1961).

k) *Gradient coupling*

Finally, we consider the interaction of a ray with a region of high gradient (Fig. 13a). Zeroth order ART predicts the ray will propagate through the region with no interaction. But if the region is narrow or the frequency low, we expect reflected and transmitted signals to be generated as for an interface (conditions in 1-dimensional models have been given in the references cited below). Including higher-order terms in ART does not generate these signals in a useful fashion. This problem has been thoroughly investigated in 1-dimensional models (Scholte, 1962; Richards and Frasier, 1976; Chapman, 1981; Kennett and Illingworth, 1981). Iterative solutions rather than asymptotic series are used. A similar technique with ART can be used in inhomogeneous models, but theoretical or numerical details do not appear to have been developed yet.

Changes in the velocity gradient also cause rapid changes in the geometrical spreading function. For instance, velocity maxima cause the spreading function to be infinite and the geometrical amplitude zero. In the next section we also discuss problems caused by gradient discontinuities.

Numerical problems with GRT

We have already described various problem signals (Figs. 8–13) that are intrinsic to the physical problem.

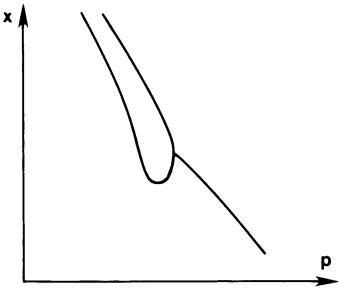

Fig. 14. The range as a function of ray parameter for rays near grazing a gradient discontinuity. For the grazing ray, $\partial_p x$ is infinite. In the figure, rays to the left of the singularity have propagated through the discontinuity. The *upper curve* corresponds to the situation when the magnitude of the gradient decreases across the discontinuity and the *lower curve* to an increase

Other difficulties arise with solutions using GRT caused by the numerical methods.

A velocity model must be specified numerically. Some features may be physically insignificant but very troublesome, i.e. gradient discontinuities. If the velocity distribution is interpolated linearly, the gradient discontinuities can cause caustics and other singularities. This is illustrated in Fig. 14, where we have plotted the range function of rays in the neighbourhood of the ray grazing the gradient discontinuity. Without going into details, it is evident from the dynamic ray equations, Eq. (20), that second-order discontinuities will cause trouble. At finite frequency these features (Fig. 14) may be too small to be resolved, but ART offers no solution.

In order to use GRT it is necessary to solve the two-point ray tracing problem, i.e. find the exact ray(s) that join the source and receiver. Various techniques have been developed, e.g. 'ray shooting' and 'ray bending', but the details need not concern us here. Suffice it to say that singularities caused by velocity gradient discontinuities will also cause difficulties when searching for the correct ray.

As a result of these numerical difficulties with the validity of ART and perturbation of rays, it is necessary to smoothly interpolate models. Velocity gradients and interface curvatures should be continuous. Various techniques have been used – specialized analytic functions or higher-order numerical methods. Spline functions are ideal but become expensive for 2- or 3-dimensional models. In 1-dimension, analytic results exist for the ray integrals for many velocity functions that can be used for interpolation. In 2- or 3-dimensions, no such general analytic results exist and we must solve the ray equations, Eqs. (13) and (20), numerically. This is often an expensive procedure as high relative accuracy of ray times is needed. At finite frequencies these efforts are essentially wasted as the waves cannot resolve the small numerical features.

Transformed equations

In the previous sections we have described some of the successes and failures of ART. In this section and the next we generalize the ideas of ART and obtain a more

versatile solution. The success of the method depends on Liouville's theorem, Eq. (21). Although the Jacobian (17) may be zero or infinite, the Jacobian of position *and* slowness is always unity. The method follows Chapman and Drummond (1982) and Thomson and Chapman (1985).

First, we define the Fourier transform with respect to spatial co-ordinates:

$$\hat{\tilde{\phi}}(\omega, \mathbf{y}) = \left(-\frac{i\omega}{2\pi}\right)^{\frac{1}{2}} \int_{-\infty}^{\infty} \hat{\phi}(\omega, \mathbf{x})\, e^{-i\omega p x}\, dx = F[\hat{\phi}] \tag{24}$$

with the inverse

$$\hat{\phi}(\omega, \mathbf{x}) = \left(\frac{i\omega}{2\pi}\right)^{\frac{1}{2}} \int_{-\infty}^{\infty} \hat{\tilde{\phi}}(\omega, \mathbf{y})\, e^{i\omega p x}\, dp = F^{-1}[\hat{\tilde{\phi}}]. \tag{25}$$

The vector $\mathbf{y}$ is the mixed vector (p, y, z). In general, this transform can be defined for any number of the coordinates, but for simplicity we restrict ourselves to one coordinate, x. Applying this transform to the wave equation (3), we obtain the transformed wave equation

$$(-\omega^2 p^2 + \nabla_\perp^2)\hat{\tilde{\phi}} + \omega^2 u^2[(-i\omega)^{-1}\partial_p, y, z]\hat{\tilde{\phi}} = 0 \tag{26}$$

where $\nabla_\perp = (0, \partial_y, \partial_z)$. The exact meaning of the second term uses the definition of the pseudo-differential operator (Hörmander, 1979; Thomson and Chapman, 1985). We attempt to solve this equation using the same technique as ART. Thus we use an ansatz

$$\hat{\tilde{\phi}}(\omega, \mathbf{y}) = \hat{\phi}_0(\omega) \sum_{n=0}^{\infty} \frac{\tilde{A}^{(n)}(\mathbf{y})}{(-i\omega)^n}\, e^{i\omega \tilde{T}(\mathbf{y})} \tag{27}$$

substitute in Eq. (26), collect terms of equal order in ω and obtain modified eikonal and transport equations. These are (from ω^2)

$$(\nabla_\perp \tilde{T})^2 - \tilde{u}^2 + p^2 = 0 \tag{28}$$

and (from ω)

$$2\nabla_\perp \tilde{A}^{(0)} \cdot \nabla_\perp \tilde{T} + \tilde{A}^{(0)} \nabla_\perp^2 \tilde{T} + \partial_p \tilde{A}^{(0)}\, d_x \tilde{u}^2 + \tfrac{1}{2}\tilde{A}^{(0)} \partial_p \partial_x \tilde{u}^2 = 0 \tag{29}$$

where $\tilde{u} = u(-\partial_p \tilde{T}, y, z)$ (Thomson and Chapman, 1985). Comparing the eikonal equations, Eqs. (7) and (28), we see that T and $\tilde{T}$ must be related by the partial Legendre transformation [Courant and Hilbert (1962), p. 35, Eqs. (7) and (8)]

$$\tilde{T}(\mathbf{y}) = T(x(\mathbf{y}), y, z) - p\, x(\mathbf{y}). \tag{30}$$

The transport equation, Eq. (29), can be solved using a suitable form of Smirnov's lemma and

$$d_v\left[\tilde{A}^{(0)2}(\mathbf{y})\left(\frac{\partial \mathbf{y}}{\partial \mathbf{x}_0}\bigg|_v\right)\right] = 0. \tag{31}$$

These results can also be obtained by connecting the asymptotic solutions, Eqs. (4) and (27), through the transform (24). Substituting the zeroth-order term from Eq. (4), $\hat{\phi}^{(0)}$ say, in Eq. (24), the phase has stationary points when

$$\partial_x T = p. \tag{32}$$

The transform variable, p, can be identified with the horizontal slowness, Eq. (9), at these points. Evaluating the Fourier transform by the stationary phase method, we find

$$F[\hat{\phi}^{(0)}] \simeq A^{(0)}(\mathbf{x}) \left|\frac{\partial x}{\partial p}\right|^{\frac{1}{2}} e^{-i\,\mathrm{sgn}(\omega)\frac{\pi}{2}\mathrm{Ind}(\partial_x^2 T) + i\omega\tilde{T}} \tag{33}$$

where all terms are evaluated at the stationary point, Eq. (32). The Morse index, Ind(...), is defined by the orientation and shape of the stationary point. In general, it is the number of negative eigenvalues of the Hessian matrix, $\partial_{x_i}\partial_{x_j} T$ (Morse lemma, Milnor, 1969, p. 6). In our case, because we have only transformed one co-ordinate, it is zero if $\partial_x^2 T = \partial_x p > 0$, and unity if $\partial_x^2 T = \partial_x p < 0$. Thus we have

$$\begin{aligned}\tilde{A}_+^{(0)}(\mathbf{y}) &= A_+^{(0)}(\mathbf{x}) \left|\frac{\partial x}{\partial p}\right|^{\frac{1}{2}} e^{-i\frac{\pi}{2}\mathrm{Ind}(\partial_x^2 T)} \\ &= A_+^{(0)}(\mathbf{x}_0) \left|\frac{\partial \mathbf{x}}{\partial \mathbf{x}_0}\bigg|_v\right|^{-\frac{1}{2}} \left|\frac{\partial x}{\partial p}\right|^{\frac{1}{2}} e^{-i\frac{\pi}{2}[\mathrm{Ind}(\partial_x^2 T) + \sigma(\mathbf{x}, \mathbf{x}_0)]}\end{aligned} \tag{34}$$

which agrees with Eq. (31). The asymptotic relationship between the zeroth-order terms in the $\mathbf{x}$- and $\mathbf{y}$-spaces has been called the asymptotic Fourier transform (AFT) by Ziolkowski and Deschamps (1984) (see also Thomson and Chapman, 1985). It can be written as

$$\hat{\tilde{\phi}}^{(0)} = F_0[\hat{\phi}^{(0)}] \tag{35}$$

where F_0 represents the second-order stationary phase evaluation of the FT and is given exactly by Eqs. (30) and (34) (with the added generality that there may be multiple stationary points or rays). Its inverse can be written

$$\hat{\phi}^{(0)} = F_0^{-1}[\hat{\tilde{\phi}}^{(0)}]. \tag{36}$$

Although expression (36) is an exact relationship, and therefore breaks down at caustics, the canonical transformation $(\partial \mathbf{y}/\partial \mathbf{x}_0)$ for $\tilde{A}^{(0)}(\mathbf{y})$ is generally finite, even at caustics where $\partial_p x = 0$. In general, this follows from Liouville's theorem, Eq. (21). In the phase space $\mathbf{x} \times \mathbf{p}$, the ray trajectories do not form caustics (Liouville's theorem – the flow is incompressible). The ray paths lie on a 3-dimensional surface in the 6-dimensional phase space and do not cross. Only when these paths are projected into $\mathbf{x}$-space are caustics formed. In $\mathbf{y}$-space, different caustics are formed. In general, if the caustic is parallel to the x-axis or if the Jacobian has a second-order zero, other transform(s) may be necessary, but Liouville's theorem guarantees that there is always a domain in which a particular point is not a caustic.

Since $\hat{\tilde{\phi}}^{(0)}$ is generally finite, it is sensible to try

$$\hat{\phi} \simeq F^{-1}[\hat{\tilde{\phi}}^{(0)}] \tag{37}$$

as an approximate solution. This is essentially Maslov's canonical operator (Maslov, 1965). This solution is still asymptotically valid and is generally finite at caustics. It reduces to the WKBJ seismogram in laterally homogeneous media (Chapman, 1978). In the next section we investigate non-asymptotic methods of evaluating Eq. (37).

Inverse transforms

In the previous section, we have obtained an asymptotic solution, Eq. (27), in a transformed domain. If the inverse transform, Eq. (25), is evaluated asymptotically, i.e. the AFT, we just obtain ART. We must evaluate the integral more accurately. The traditional method is to use higher-order asymptotic methods, e.g. the third-order saddle point method, the incomplete saddle point method etc., or to compute the integral numerically. These methods are called *spectral* methods (Chapman, 1978) as the intermediate result is $\hat{\phi}(\omega, \mathbf{x})$. The analytic techniques lack generality and the numerical methods are expensive at high frequencies. An alternative approach, the *slowness* methods, is preferable.

Combining the inverse frequency and slowness integrals, Eqs. (2) and (25), reversing the order of integration and evaluating the frequency integral first, we obtain

$$\phi(t, \mathbf{x}) = -\frac{1}{2^{\frac{1}{2}}\pi}\, \partial_t \bar{\lambda}(t) * \int_{-\infty}^{\infty} \tilde{\phi}(t - px, \mathbf{y})\, dp \tag{38}$$

$$\left[(i\omega/2\pi)^{\frac{1}{2}} = -\frac{1}{2^{\frac{1}{2}}\pi}(-i\omega)(\pi/|\omega|)^{\frac{1}{2}}\, e^{-i\,\mathrm{sgn}(\omega)\frac{\pi}{4}}\right].$$

A product in the frequency domain has become a convolution in the time domain. The time series, $\lambda(t) = H(t)\, t^{-\frac{1}{2}}$, has a spectrum

$$\hat{\lambda}(\omega) = \left(\frac{\pi}{|\omega|}\right)^{\frac{1}{2}} e^{i\,\mathrm{sgn}(\omega)\frac{\pi}{4}} \tag{39}$$

and the Hilbert transform is $\bar{\lambda}(t) = H(-t)(-t)^{-\frac{1}{2}}$. We can also take the inverse frequency transform of the spatial transform, Eq. (24), and obtain

$$\tilde{\phi}(t, \mathbf{y}) = \frac{1}{2^{\frac{1}{2}}\pi}\, \partial_t \lambda(t) * \int_{-\infty}^{\infty} \phi(t + px, \mathbf{y})\, dx. \tag{40}$$

These results, Eqs. (38) and (40), can be recognized as a Radon transform pair (Chapman, 1978), the latter being commonly known as *slant stacking*.

Using the zeroth term in the asymptotic series (27), we obtain the simple result

$$\tilde{\phi}^{(0)}(t, \mathbf{y}) = \mathrm{Re}\,\{\tilde{A}_+^{(0)}(\mathbf{y})\, \Phi_0[t - \tilde{T}(\mathbf{y})]\} \tag{41}$$

analogous to Eq. (5) with $n = 0$. Substitute Eq. (41) in Eq. (38) and we have

$$\phi(t, \mathbf{x}) = -\frac{1}{2^{\frac{1}{2}}\pi}\, \phi_0(t) * \partial_t \bar{\lambda}(t) * \mathrm{Re} \int_{-\infty}^{\infty} \tilde{A}_+^{(0)}(\mathbf{y})\, \Delta[t - \tilde{\theta}(p, \mathbf{x})]\, dp \tag{42}$$

where $\Delta(t) = \delta(t) - i/\pi t$, the analytic delta function, and

$$\tilde{\theta}(p, \mathbf{x}) = \tilde{T}(\mathbf{y}) + px. \tag{43}$$

Expanding the complex terms and transferring the Hilbert transform operator through the convolution operator, we obtain

$$\phi(t, \mathbf{x}) = -\frac{1}{2^{\frac{1}{2}}\pi}\, \phi_0(t) * \partial_t \,\mathrm{Im}\left[\Lambda(t) * \int_{-\infty}^{\infty} \tilde{A}_+^{(0)}(\mathbf{y})\, \delta(t - \tilde{\theta})\, dp\right]. \tag{44}$$

Evaluating the integral at the singularities of the delta function, we have

$$\phi(t, \mathbf{x}) = -\frac{1}{2^{\frac{1}{2}}\pi}\, \phi_0(t) * \partial_t \,\mathrm{Im}\left[\Lambda(t) * \sum_{t=\tilde{\theta}} \frac{\tilde{A}_+^{(0)}(\mathbf{y})}{|\partial_p \tilde{\theta}|}\right] \tag{45}$$

where the final summation includes all p's that solve

$$t = \tilde{\theta}(p, \mathbf{x}). \tag{46}$$

Note that evaluation of the inverse integrals is exact, provided $\tilde{T}(\mathbf{y})$ is real. No approximation beyond Eq. (41) is made. However, for some p's, $\tilde{T}(\mathbf{y})$ is complex and hence the complete integrals in Eqs. (42) and (44) should be approximated by a restricted range. In the later section on 'Smoothing' [b) attenuation and c) Gaussian beam method] we discuss some cases when $\tilde{T}(\mathbf{y})$ is complex.

Expression (45) has become known as the WKBJ seismogram (1-dimensional models; Chapman, 1978) or the Maslov seismogram (2- or 3-dimensional models; Chapman and Drummond, 1982). It is extremely easy to evaluate and widely applicable. Only the results of kinematic Eq. (13) and dynamic Eq. (20) ray tracing are needed. It is a special, limiting case of the Gaussian beam method (infinite beam width). In the next section we shall use it to investigate the canonical problems.

The convolution operator, $\Lambda(t) = \lambda(t) + i\bar{\lambda}(t)$, is easy to evaluate as the imaginary part is simply the time reversal of the real part. A simple rational approximation has been given by Chapman and Drummond (1982). Alternatively the convolution can be performed in the frequency domain. Nevertheless, as we shall see in the next section, the construct for some signals, e.g. reflections, is strange. Two acausal signals are convolved and give a causal result. Taking the Hilbert transform of both signals would give a more natural construction. An alternative slowness method with complex p values provides this. We must be more careful now to consider whether $\omega \gtrless 0$, which we indicate with subscripts $\pm$. The method closely follows Heyman and Felsen (1984). We proceed as before and evaluate the frequency integral first but consider the positive and negative frequencies separately. We obtain

$$\phi(t, \mathbf{x}) = \frac{1}{2^{\frac{3}{2}}\pi^2}\, \phi_0(t) * \partial_t \lambda(t) * \left\{\int_{C_+} \frac{\tilde{A}_+^{(0)}(\mathbf{y})}{t - \tilde{\theta}_+}\, dp + \int_{C_-} \frac{\tilde{A}_-^{(0)}(\mathbf{y})}{t - \tilde{\theta}_-}\, dp\right\} \tag{47}$$

where the contours $C_\pm$ lie infinitesimally above or below the p real axis (depending on $\partial_p \tilde{\theta} \gtrless 0$ and $\omega \gtrless 0$, Fig. 15) so that $\mathrm{Im}(\tilde{\theta}_\pm) \gtrless 0$. We have used

$$\int_0^{\infty} e^{i\omega(\tilde{\theta}_+ - t)}\, d\omega = -i/(t - \tilde{\theta}_+),$$

$$\int_{-\infty}^{0} e^{i\omega(\tilde{\theta}_- - t)}\, d\omega = i/(t - \tilde{\theta}_-).$$

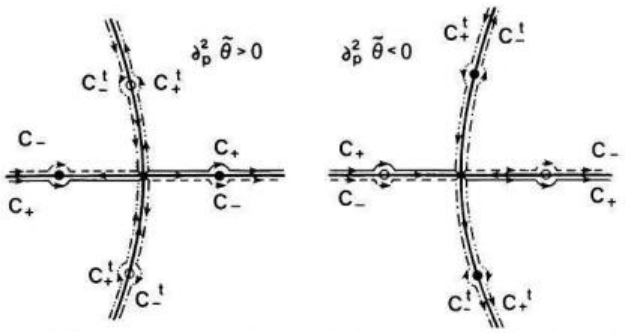

Fig. 15. The contours $C_\pm$ and $C'_\pm$ in the neighbourhood of stationary points where $\partial_p^2\tilde{\theta}\gtrless 0$. The *open circles* are poles for t less than the saddle point values and the *closed circles* are for t greater than this value. The contours $C_\pm$ are distorted to $C'_\pm$ through the corresponding valley of the saddle point

If $\tilde{A}_+^{(0)}$ is real on the real axis, $\tilde{A}_+^{(0)}=\tilde{A}_-^{(0)}$. The integrals loop in opposite directions about the poles, Eq. (46), on the real axis, and the half-loops cancel. On the real axis, the integrals double up and we obtain the Cauchy principal value, i.e.

$$\phi(t,\mathbf{x})=\frac{1}{2^{\frac{1}{2}}\pi^2}\,\phi_0(t)*\partial_t\lambda(t)*P\int_{-\infty}^{\infty}\frac{\tilde{A}_+^{(0)}(\mathbf{y})}{t-\tilde{\theta}}\,dp. \tag{48}$$

The integral can be rewritten as a convolution integral and recognized as the Hilbert transform. Transferring the Hilbert transform to $\lambda(t)$, we obtain the WKBJ result, Eq. (45), for the real part. Alternatively, we can distort the contours $C_\pm$ to the complex contours $C'_\pm$ defined by Eq. (46) with t varying. The situation differs for $\partial_p^2\tilde{\theta}\gtrless 0$ and $\omega\gtrless 0$ (Fig. 15), but in both cases the contours $C'_\pm$ run in opposite directions and cancel except for the loops around the poles. The result is

$$\phi(t,\mathbf{x})=-\frac{2^{\frac{1}{2}}}{\pi}\,\phi_0(t)*\partial_t\lambda(t)*\mathrm{Im}\left\{\frac{\tilde{A}_+^{(0)}(\mathbf{y})}{\partial_p\tilde{\theta}_+}\right\}_{t=\tilde{\theta}} \tag{49}$$

where we take the pole below the axis. This result is variously called the generalized ray method or the Cagniard-de Hoop-Pekeris method (Cagniard, 1939, 1962; Pekeris, 1955a, b; de Hoop, 1960), but this derivation, due to Heyman and Felsen (1984), is valid for $\partial_p^2\tilde{\theta}\gtrless 0$ not just $\partial_p^2\tilde{\theta}<0$.

If $\tilde{A}_+^{(0)}(\mathbf{y})$ is imaginary on the real axis, $\tilde{A}_+^{(0)}=-\tilde{A}_-^{(0)}$. The integrals (47) on the real axis cancel and the half loops about the poles (46) combine to give residues. The loop direction depends on $\partial_p\tilde{\theta}\gtrless 0$ (Fig. 15). Hence we obtain

$$\phi(t,\mathbf{x})=\frac{1}{2^{\frac{1}{2}}\pi}\,\phi_0(t)*\partial_t\lambda(t)*\sum_{t=\tilde{\theta}}\frac{i\tilde{A}_+^{(0)}}{|\partial_p\tilde{\theta}|} \tag{50}$$

in agreement with Eq. (45). Result (49) can be generalized to include the case when $\tilde{A}^{(0)}$ has an imaginary part due to a branch cut, i.e. total reflection.

As mentioned above, expression (49) may lead to a more natural construction for signals involving Hilbert transforms. Another advantage is that we are not restricted to p and $\tilde{T}$ real and, therefore, end-point errors from a restricted p range will not occur. Nevertheless, these advantages may be outweighed by the difficulties of analytically continuing the required functions in the complex p-domain. If the functions are defined analytically, the continuation is automatic but for numerical approximations the process is unstable. The Cagniard-de Hoop-Pekeris method has been widely used in models of homogeneous layers, but not in more general inhomogeneous structures.

End-point errors occur in the WKBJ/Maslov seismograms, Eq. (45), due to the restricted p range used. Effectively, the amplitude function, $\tilde{A}^{(0)}(\mathbf{y})$, is taken zero in the range where $\tilde{T}(\mathbf{y})$ is complex. The discontinuity in the amplitude causes end-point arrivals. These arrivals can be removed by tapering the amplitude function smoothly at the end-points. This procedure is purely cosmetic and may introduce other errors. An alternative is to estimate the part of the p-integral ignored by some simple analytic technique (Thomson and Chapman, in preparation). Let us consider the simplest case where $\tilde{A}^{(0)}(\mathbf{y})$ and $\partial_p\tilde{\theta}$ are finite and non-zero at the end-points. The integrals (42) and (44) are restricted to the range $p_1\leqq p\leqq p_2$, say. Thus the complete result is (Thomson and Chapman, in preparation)

$$\begin{aligned}\phi(t,\mathbf{x})&=\frac{1}{2\pi}\int_B\left(\frac{i\omega}{2\pi}\right)^{\frac{1}{2}}\left(\int_{-\infty}^{p_1}+\int_{p_1}^{p_2}+\int_{p_2}^{\infty}\right)\hat{\phi}_0(\omega)\,\tilde{A}^{(0)}(\mathbf{y})\\&\quad\cdot e^{i\omega[\tilde{\theta}(p_0\mathbf{x})-t]}\,dp\,d\omega\\&=\int_{p_1}^{p_2}\frac{1}{2\pi}\int_B\left(\frac{i\omega}{2\pi}\right)^{\frac{1}{2}}\hat{\phi}_0(\omega)\,\tilde{A}^{(0)}(\mathbf{y})\\&\quad\cdot e^{i\omega[\tilde{\theta}(p,\mathbf{x})-t]}\,d\omega\,dp\\&\quad+\frac{1}{2\pi}\int_B\left(\frac{i\omega}{2\pi}\right)^{\frac{1}{2}}\hat{\phi}_0(\omega)\,\tilde{A}^{(0)}(\mathbf{y})\\&\quad\cdot\frac{e^{i\omega[\tilde{\theta}(p,\mathbf{x})-t]}}{i\omega\,\partial_p\theta}\Bigg|_{-\infty}^{p_1}+\Bigg|_{p_2}^{\infty}d\omega+\ldots\\&\simeq-\frac{1}{2^{\frac{1}{2}}\pi}\,\phi_0(t)\\&\quad*\partial_t\,\mathrm{Im}\left\{\Lambda(t)*\left[\sum_{t=\tilde{\theta}}\frac{\tilde{A}_+^{(0)}(\mathbf{y})}{|\partial_p\tilde{\theta}|}\right.\right.\\&\quad-\frac{\tilde{A}_+^{(0)}(\mathbf{y})}{\partial_p\tilde{\theta}}\Bigg|_{p_1}H(t-\tilde{\theta}(p_1,\mathbf{x}))\\&\quad\left.\left.+\frac{\tilde{A}_+^{(0)}(\mathbf{y})}{\partial_p\tilde{\theta}}\Bigg|_{p_2}H(t-\tilde{\theta}(p_2,\mathbf{x}))\right]\right\}.\end{aligned} \tag{51}$$

The first term in expression (51) is, of course, the original WKBJ result, Eq. (45). The other terms are obtained by evaluating the semi-infinite integrals by parts. Only the lowest-order term is retained: higher-order terms, involving derivatives of $\tilde{A}^{(0)}$ and $\partial_p\tilde{\theta}$ can be obtained by further integrations. It is easily seen that, to lowest order, the end-point arrivals in the WKBJ seismogram (45) are cancelled by the new terms in Eq. (51). In other situations we must consider the case where $\tilde{A}^{(0)}(\mathbf{y})$ and $\tilde{\theta}$ have singularities, e.g. square root, at the end points (Thomson and Chapman, in preparation).

Canonical problems

In this section we use the results from the last section to investigate some of the canonical problems described earlier.

a) *Direct rays*

The travel-time for typical direct rays is illustrated in Fig. 4b. The slope of the curve is the horizontal slowness p, Eq. (9), and the intercept is the time $\tilde{T}$, Eq. (30). The Legendre transformation is illustrated in Fig. 4c. The slope of the curve, $\tilde{T}$, is $-x$ and the intercept is T. For a normal direct ray $\partial_x^2 T > 0$.

In evaluating the seismogram (45) we need

$$\partial_p \tilde{\theta} = x - x(\mathbf{y}). \tag{52}$$

This function is zero for the ray parameter, p_{ray}, which solves the two-point ray tracing problem, i.e. $x = x(\mathbf{y}_{\text{ray}})$. At this point, the function $\tilde{\theta}$ reduces to the travel-time, i.e. $T(\mathbf{x}) = \tilde{\theta}(p_{\text{ray}}, \mathbf{x})$ when $x = x(\mathbf{y}_{\text{ray}})$. In constructing the seismogram (45), we need to know the form of $\tilde{A}^{(0)}(\mathbf{y})$ and the shape of $\tilde{\theta}(p, \mathbf{x})$, i.e. the sign of $\partial_p^2 \tilde{\theta} = -\partial_p x$, as

$$t = \tilde{\theta}(p, \mathbf{x}) \simeq T(\mathbf{x}) + \tfrac{1}{2}\partial_p^2 \tilde{\theta}(p - p_{\text{ray}})^2 \tag{53}$$

Now $\partial_x^2 T > 0$ so the Morse index is zero and $\tilde{A}^{(0)}(\mathbf{y})$ real and $\partial_p^2 \tilde{\theta} < 0$. The construction of the seismogram reduces to (Fig. 4d)

$$\begin{aligned}\phi(t, \mathbf{x}) &\simeq -\frac{1}{2^{\frac{1}{2}}\pi}\, \phi_0(t) * \partial_t \left[\bar{\lambda}(t) * \frac{2\tilde{A}_+^{(0)}(\mathbf{y})}{\sqrt{2(\partial_p x)(T-t)}}\right] \\ &= A_+^{(0)}(\mathbf{x})\, \phi_0(t-T)\end{aligned} \tag{54}$$

using Eq. (34) and $\bar{\lambda}(t) * \bar{\lambda}(t) = -\pi H(t)$. This agrees with ART, Eq. (5), but the exact evaluation of Eq. (45) will include variations in $\tilde{A}^{(0)}(\mathbf{y})$ and $(\partial_p x)$ away from the stationary point. This is an example where the alternative Cagniard form, Eq. (49), is simpler. Then

$$\phi(t, \mathbf{x}) \simeq -\frac{2^{\frac{1}{2}}}{\pi}\, \phi_0(t) * \partial_t \left[\lambda(t) * -\frac{\tilde{A}_+^{(0)}(\mathbf{y})}{\sqrt{2(\partial_p x)(t-T)}}\right.$$

which reduces to Eq. (54). In this case $\partial_p \tilde{\theta}_+$ is positive imaginary below the saddle point.

b) *Normal turning rays*

The travel time for typical normal turning rays is illustrated in Fig. 5b and the Legendre transformation in Fig. 5c. For a normal turning ray, $\partial_x^2 T < 0$, so the Morse index is unity and $\tilde{A}^{(0)}(\mathbf{y})$ imaginary, and $\partial_p^2 \tilde{\theta} > 0$. Thus the construction of the seismogram reduces to (Fig. 5d).

$$\begin{aligned}\phi(t, \mathbf{x}) &\simeq -\frac{1}{2^{\frac{1}{2}}\pi}\, \phi_0(t) * \partial_t \left(\lambda(t) * \frac{2\,\mathrm{Im}\,[\tilde{A}_+^{(0)}(\mathbf{y})]}{\sqrt{-2(\partial_p x)(t-T)}}\right) \\ &= A_+^{(0)}(\mathbf{x})\, \phi_0(t-T)\end{aligned} \tag{55}$$

using Eq. (34) and $\lambda(t) * \lambda(t) = \pi H(t)$. This agrees with ART, Eq. (5), but the exact evaluation of Eq. (45) will include variations in $\tilde{A}^{(0)}(\mathbf{y})$ and $(\partial_p x)$ away from the stationary point.

For multiple turning rays, e.g. PP, the situation changes as typically a caustic exists. If $\partial_p^2 \tilde{\theta} > 0$, i.e. normal, the Morse index is unity, but so is the KMAH index. $\tilde{A}^{(0)}(\mathbf{y})$ is real and opposite in sign to $A^{(0)}(\mathbf{x})$. Hence the seismogram is

$$\begin{aligned}\phi(t, \mathbf{x}) &\simeq -\frac{1}{2^{\frac{1}{2}}\pi}\, \phi_0(t) * \partial_t \left(\bar{\lambda}(t) * \frac{2\tilde{A}_+^{(0)}(\mathbf{y})}{\sqrt{-2(\partial_p x)(t-T)}}\right) \\ &= -\,\mathrm{Im}\,[A_+^{(0)}(\mathbf{x})]\, \bar{\phi}_0(t-T)\end{aligned} \tag{56}$$

agreeing with Eq. (5). As expected, we obtain the Hilbert transform of the direct pulse. As the final result contains a Hilbert transform there is not much to choose between Eqs. (45) and (49).

c) *Reversed turning rays*

For a reversed ray, a caustic exists. The KMAH index is unity but the Morse index is zero ($\partial_p^2 \tilde{\theta} < 0$) (Fig. 6). Thus $\tilde{A}^{(0)}(\mathbf{y})$ is imaginary and the seismogram is constructed

$$\begin{aligned}\phi(t, \mathbf{x}) &\simeq -\frac{1}{2^{\frac{1}{2}}\pi}\, \phi_0(t) * \partial_t \lambda(t) * \frac{2\,\mathrm{Im}\,[\tilde{A}_+^{(0)}(\mathbf{y})]}{\sqrt{2(\partial_p x)(T-t)}} \\ &= -\,\mathrm{Im}\,[A_+^{(0)}(\mathbf{x})]\, \bar{\phi}_0(t-T).\end{aligned} \tag{57}$$

As expected, we obtain the Hilbert transform. For a multiple turning ray on a reversed branch, the KMAH index is two and the Morse index zero. Thus we get

$$\begin{aligned}\phi(t, \mathbf{x}) &\simeq -\frac{1}{2^{\frac{1}{2}}\pi}\, \phi_0(t) * \partial_t \bar{\lambda}(t) * \frac{2\tilde{A}_+^{(0)}(\mathbf{y})}{\sqrt{2(\partial_p x)(T-t)}} \\ &= A_+^{(0)}(\mathbf{x})\, \phi_0(t-T).\end{aligned} \tag{58}$$

$A^{(0)}(\mathbf{x})$ and $\tilde{A}^{(0)}(\mathbf{y})$ have the opposite sign to $A^{(0)}(\mathbf{x}_0)$ so the pulse is inverted. This is another example where the alternative formulation, Eq. (49), may be advantageous.

d) *Reflected and transmitted rays*

Normally, unless caustics are present, the travel-time curves for reflections and transmissions are as reversed rays, $\partial^2 T > 0$ (Fig. 7). The amplitude functions, $A^{(0)}(\mathbf{x})$ and $\tilde{A}^{(0)}(\mathbf{y})$, may be real (partial reflections) or complex (total reflections). With these generalities, we obtain

$$\begin{aligned}\phi(t, \mathbf{x}) &\simeq -\frac{1}{2^{\frac{1}{2}}\pi}\, \phi_0(t) * \partial_t\, \mathrm{Im}\left[A(t) * \frac{2\tilde{A}_+^{(0)}(\mathbf{y})}{\sqrt{2(\partial_p x)(T-t)}}\right] \\ &= \mathrm{Re}\,\{A_+^{(0)}(\mathbf{x})\, \Phi_0(t-T)\}\end{aligned} \tag{59}$$

in agreement with Eq. (5). Note that the real part of $\tilde{A}_+^{(0)}(\mathbf{y})$ is convolved with $\bar{\lambda}(t)$, an awkward construction with two Hilbert transforms, whereas the imaginary part is convolved with $\lambda(t)$. The alternative construction (49) is

$$\begin{aligned}\phi(t, \mathbf{x}) &\simeq -\frac{2^{\frac{1}{2}}}{\pi}\, \phi_0(t) * \partial_t \lambda(t) \\ &\quad * \left\{-\frac{\mathrm{Re}\,[\tilde{A}_+^{(0)}(\mathbf{y})]}{\sqrt{2(\partial_p x)(t-T)}} + \frac{\mathrm{Im}\,[\tilde{A}_+^{(0)}(\mathbf{y})]}{\sqrt{2(\partial_p x)(T-t)}}\right\}\end{aligned} \tag{60}$$

and the real part of $\tilde{A}_+^{(0)}(\mathbf{y})$ contributes off the real axis.

e) *Critical rays and head waves*

The head wave is caused by a square root singularity at the branch point in a reflection/transmission coefficient in $\tilde{A}_+^{(0)}(\mathbf{y})$. Suppose this occurs due to a square root, q_h, contained in $\tilde{A}_+^{(0)}(\mathbf{y})$ which is zero at $p = p_h$ (q_h would be

a slowness component perpendicular to the interface). Then we define

$$l_h = \partial_p \tilde{\theta}(p_h, \mathbf{x}) = x - x(p_h) \tag{61}$$

as the length of the head wave ($x_h = x(p_h)$ is the critical range). The arrival time of the head wave is (Fig. 8)

$$t_h = \tilde{\theta}(p_h, \mathbf{x}) = T(x_h) + p_h l_h. \tag{62}$$

Expanding about the branch point, from Eq. (45) we obtain (if $l_h > 0$)

$$\begin{aligned}\phi(t, \mathbf{x}) &\simeq -\frac{1}{2^{\frac{1}{2}}\pi}\phi_0(t) * \partial_{q_h}\tilde{A}_+^{(0)}(\mathbf{y})\left(\frac{2p_h}{l_h^3}\right)^{\frac{1}{2}} \\ &\quad \cdot \partial_t[\lambda(t) * (t-t_h)^{\frac{1}{2}} + \bar{\lambda}(t) * (t_h - t)^{\frac{1}{2}}] \\ &= \frac{p_h^{\frac{1}{2}}}{l_h^{\frac{1}{2}}}\partial_{q_h}\tilde{A}_+^{(0)}(\mathbf{y})\,\phi_0(t-t_h) * H(t)\end{aligned} \tag{63}$$

(where we ignore the constant part of $\tilde{A}_+^{(0)}(\mathbf{y})$) i.e. the integral of the direct pulse. Note that in the final time series in Eq. (45), points with $p < p_h$ contribute to $t < t_h$, and $p > p_h$ to $t > t_h$. If $l_h < 0$ the situation is reversed and we obtain

$$\begin{aligned}\phi(t, \mathbf{x}) &\simeq -\frac{1}{2^{\frac{1}{2}}\pi}\phi_0(t) * \partial_{q_h}\tilde{A}^{(0)}(\mathbf{y})\left(\frac{2p_h}{-l_h^3}\right)^{\frac{1}{2}} \\ &\quad \cdot \partial_t[\lambda(t) * (t_h - t)^{\frac{1}{2}} + \bar{\lambda}(t) * (t - t_h)^{\frac{1}{2}}] \\ &= 0.\end{aligned}$$

Using the alternative formulation (49), the contribution comes from the part of the contour $C_{\pm}^t$ looping around the branch cut, i.e. only if $l_h > 0$ and then only from $p > p_h$. Taking this contribution we obtain

$$\begin{aligned}\phi(t, \mathbf{x}) &= -\frac{2^{\frac{1}{2}}}{\pi}\phi_0(t) \\ &\quad * \partial_t\left[\lambda(t) * \partial_{q_h}\tilde{A}_+^{(0)}(\mathbf{y})\left(\frac{2p_h}{l_h^3}\right)^{\frac{1}{2}}(t-t_h)^{\frac{1}{2}}\right]\end{aligned} \tag{64}$$

which reduces to Eq. (63). Note that this construction is more convenient as the result is not divided equally between two terms, one of which has two Hilbert transforms. Similarly for $l_h < 0$, we do not depend on the cancellation of two equal and opposite terms.

The head wave, Eq. (63), is the integral of the direct pulse and can be derived using first-order asymptotic theory, i.e. $A^{(1)}(\mathbf{x})$, as $A^{(0)}(\mathbf{x})$ is zero (Červený and Ravindra, 1971). At the critical point, x_h, the head wave diverges as $l_h = 0$. Both formulations, Eqs. (45) and (49), remain valid in the neighbourhood of the critical point: the alternative formulation (49) is more direct. The resultant waveform is presumably equal to the inverse Fourier transform of the Weber function (Marks and Hron, 1977) although this has not been proved directly.

f) *Interference head wave*

The travel times for the multiple refractions and the reflection that contribute to the interference head wave are illustrated in Fig. 9. The expression (45) can be used to describe each ray and includes the phase changes due to multiple turning points, etc. The refractions all have an end-point at $p = p_h$. The accuracy of summing all these ray contributions to model the interference head wave has not been investigated in detail.

g) *Airy caustic*

The travel times for a caustic are illustrated in Fig. 10. Essentially, we have a normal and reversed ray in close proximity. The function $\tilde{\theta}$ is approximately cubic

$$\tilde{\theta}(p, \mathbf{x}) \simeq \tilde{\theta}(p_a, \mathbf{x}) + l_a(p - p_a) - \tfrac{1}{6}\partial_p^2 x(p - p_a)^3 \tag{65}$$

where we define the distance from the caustic

$$l_a = x - x(p_a) \tag{66}$$

and the time

$$t_a = \tilde{\theta}(p_a, \mathbf{x}) = T(p_a) + l_a p_a. \tag{67}$$

The seismogram is constructed from (Fig. 10d)

$$\begin{aligned}\phi(t, \mathbf{x}) &\simeq -\frac{1}{2^{\frac{1}{2}}\pi}\phi_0(t) * \partial_t\lambda(t) * \frac{\mathrm{Im}\,[\tilde{A}_+^{(0)}(\mathbf{y})]}{|\partial_p\tilde{\theta}|} \\ &= -\frac{3^{\frac{1}{3}}2^{\frac{1}{2}}}{\pi}\phi_0(t - t_a) \\ &\quad * \frac{\mathrm{Im}\,[\tilde{A}_+^{(0)}(\mathbf{y})]}{(\partial_p^2 x)^{\frac{1}{3}}}\partial_t C\left[t, \frac{2l_a}{3^{\frac{2}{3}}(\partial_p x)^{\frac{1}{3}}}\right]\end{aligned} \tag{68}$$

if $\partial_p^2 x > 0$. The function $C(t, y)$ is

$$C(t, y) = \int_{(\ )>0} \frac{dz}{(t - 3yz + 4z^3)^{\frac{1}{2}}} \tag{69}$$

and has been investigated in detail by Burridge (1963a, b) and Stickler et al. (1981). It can be expressed in terms of the complete elliptic integrals. Only three distinct cases need be considered, $C(t, \pm 1)$ and $C(t, 0)$, as others can be obtained by scaling (Fig. 10d).

h) *Fresnel diffraction*

The travel-time curves for a Fresnel shadow are illustrated in Fig. 12. It corresponds to a normal turning ray with an end-point, $p = p_e$. Defining the distance from the shadow edge

$$l_e = x - x(p_e) \tag{70}$$

and the diffraction arrival time

$$t_e = \tilde{\theta}(p_e, \mathbf{x}) = T(x_e) + p_e l_e \tag{71}$$

we obtain the seismogram (Fig. 12)

$$\begin{aligned}\phi(t, \mathbf{x}) &\simeq -\frac{1}{2^{\frac{1}{2}}\pi}\phi_0(t) \\ &\quad * \partial_t\left(\lambda(t) * \frac{\mathrm{Im}\,[\tilde{A}_+^{(0)}(\mathbf{y})][2 - H(t - t_e)]}{\sqrt{-2(\partial_p x)(t - T)}}\right) \\ &= A_+^{(0)}(x_e)\left[\phi_0(t - T) - \phi_0(t - t_e)\right. \\ &\quad \left. * \frac{\lambda(t)(t_e - T)^{\frac{1}{2}}}{2\pi(t + t_e - T)}\right] \quad \text{if } l_e < 0 \\ &= A_+^{(0)}(x_e)\,\phi_0(t - t_e) \\ &\quad * \frac{\lambda(t)(t_e - T)^{\frac{1}{2}}}{2\pi(t + t_e - T)} \quad \text{if } l_e > 0.\end{aligned} \tag{72}$$

If $l_e=0$, it reduces to half the geometrical amplitude, Eq. (55).

i) *Edge and point diffractions*

j) *Interface diffractions*

k) *Gradient coupling*

The extension of ART developed in the previous sections in no way models these signals. They require a more complicated solution of the wave equation containing more physics, e.g. the correct boundary conditions. The kinematic properties of the first two signals can be simulated by replacing the discontinuities by high velocity gradients. As the interaction of the wave with this gradient is not modelled, we can not expect the amplitude to be accurate. The last signal can be simulated by introducing small discontinuities. Provided the gradient is fairly uniform this will be reasonably accurate, but if the curvature is large, zeroth-order asymptotics will break down.

Smoothing

In the previous section we have discussed the construction of various signals. The time series involved have singularities and for numerical purposes it is necessary to smooth them. Chapman and Drummond (1982) have discussed a suitable smoothed, rational approximation for the convolution operator, $\partial_t \Lambda *$. Various methods can be used to smooth the other terms.

a) *Box-car smoothing*

The simplest method is to smooth the time series using a simple box-car, $2\Delta t$ long (so the spectrum is zero at the Nyquist frequency). We denote the box-car by $B(t) = \frac{1}{2}\{H(t+1)-H(t-1)\}$. Then the smoothed seismogram [from Eq. (44)]

$$\begin{aligned}&\phi(t,\mathbf{x}) * B(t/\Delta t)/\Delta t\\ &= -\frac{1}{2^{\frac{1}{2}}\pi}\phi_0(t) * \partial_t \operatorname{Im}\left\{\Lambda(t) * \int_{-\infty}^{\infty} \tilde{A}_+^{(0)}(\mathbf{y}) \frac{B[(t-\tilde{\theta})/\Delta t]}{\Delta t}\, dp\right\}\\ &= -\frac{1}{2^{\frac{1}{2}}\pi\Delta t}\phi_0(t) * \partial_t \operatorname{Im}\left[\Lambda(t) * \int_{t=\tilde{\theta}\pm\Delta t} \tilde{A}_+^{(0)}(\mathbf{y})\, dp\right]. \qquad (73)\end{aligned}$$

The final integral is evaluated over p-bands defined by the solutions of $t=\tilde{\theta}(p,\mathbf{x})\pm\Delta t$. As $\tilde{A}_+^{(0)}(\mathbf{y})$ normally varies slowly, the integrals are easily approximated.

The importance of this smoothing for any numerical algorithm cannot be overemphasized. To evaluate $|\partial_p\tilde{\theta}|^{-1}$ numerically would be unstable. To evaluate Eq. (73) numerically is simple and stable. Small features in $\tilde{\theta}(p,\mathbf{x})$ which may be due to numerical errors or artefacts, e.g. velocity gradient discontinuities in the model, do not affect the results unduly. Thus no intermediate results need be calculated more accurately than the digitization and band-limiting requires. Cruder numerical models can be used.

Expression (49) should be smoothed similarly, i.e.

$$\begin{aligned}&\phi(t,\mathbf{x}) * B(t/\Delta t)/\Delta t\\ &= -\frac{2^{\frac{1}{2}}}{\pi\Delta t}\phi_0(t) * \partial_t\lambda(t) * \int_{t=\tilde{\theta}\pm\Delta t} \operatorname{Im}(\tilde{A}_+^{(0)}(\mathbf{y})\, dp). \qquad (74)\end{aligned}$$

b) *Attenuation*

The ART ansatz only applies in non-attenuating media. In general, attenuation must be included. The zeroth-order term is then

$$\hat{\tilde{\phi}}^{(0)}(\omega,\mathbf{y}) = \tilde{A}^{(0)}(\mathbf{y})\, e^{i\omega\tilde{T}(\mathbf{y})-|\omega|t^*(\mathbf{y})} \qquad (75)$$

where we have included the simplest form of attenuation. The function, $t^*(\mathbf{y})$, is defined by

$$t^*(\mathbf{y}) = \int_{s_0}^{s} \frac{ds}{2Q(s)\,v(s)} \qquad (76)$$

where $Q(s)$ is the quality factor. The result (44) is then replaced by

$$\begin{aligned}\phi(t,\mathbf{x}) = &-\frac{1}{2^{\frac{1}{2}}\pi}\phi_0(t)\\ &* \partial_t \operatorname{Im}\left[\Lambda(t) * \int_{-\infty}^{\infty} \frac{1}{\pi}\cdot\frac{\tilde{A}_+^{(0)}(\mathbf{y})\, t^*(\mathbf{y})}{(t-\tilde{\theta})^2+t^{*2}}\, dp\right] \qquad (77)\end{aligned}$$

where the integrand is the inverse Fourier transform of $e^{-|\omega|t^*}$. Unfortunately, this integral cannot be evaluated analytically. If the attenuation varies little with ray parameter it can be factored outside the integral and included in the previous result (45) as a convolution operator. Otherwise the integral (77) must be evaluated numerically.

The simple form of attenuation, Eq. (75), is acausal. More complicated, dispersive, causal attenuation models can be used but an analytic form for the inverse Fourier transform may not be known.

c) *Gaussian beam method*

The Gaussian beam method is another technique for smoothing the results and, in as much as it does not correspond to any physical process, is more complicated. The ansatz of ART is generalized to include a Gaussian weighting about the geometrical ray, i.e. $\tilde{T}$ in Eq. (30) is replaced by

$$\tilde{T}(\mathbf{y},\delta) = \tilde{T}(\mathbf{y}) + \tfrac{1}{2}N(\mathbf{x},\delta)[x-x(\mathbf{y})]^2 \qquad (78)$$

The function, $N(\mathbf{x},\delta)$, is a complex function. More details and references can be found in Madariaga (1984). The parameter δ is related to the beam width. Following Madariaga (1984), δ is imaginary and as $\delta\to 0$, $N(\mathbf{x},\delta)\to 0$ and we have an infinite beam width. The amplitude function is also modified, $\tilde{A}^{(0)}(\mathbf{y},\delta)$, and depends on the beam parameter. Proceeding as before with the inverse transforms, we obtain

$$\begin{aligned}\phi(t,\mathbf{x}) = &-\frac{1}{2^{\frac{1}{2}}\pi}\phi_0(t) * \partial_t\bar{\lambda}(t)\\ &* \int_{-\infty}^{\infty} \operatorname{Im}\left[\frac{\tilde{A}_+^{(0)}(\mathbf{y},\delta)}{t-\tilde{\theta}(p,\mathbf{x},\delta)}\right] dp. \qquad (79)\end{aligned}$$

As $\tilde{\theta}(p,\mathbf{x},\delta)$ is complex [derived from Eq. (78) in the obvious fashion], we obtain a result not dissimilar to Eq. (77) except that the integrand broadens away from the geometrical ray parameter, i.e. the broadening is a function of the receiver location. The parameter δ is a

smoothing parameter (δ^{-1} relates to beam width). As δ increases, the beam width narrows and only those ray parameters close to the geometrical ray contribute significantly.

A numerical model

In the previous section we have seen that small features in the seismograms, i.e. compared with Δt, are automatically smoothed out in the expression (73). As a result, numerical difficulties are avoided. Also two-point ray tracing is not necessary to evaluate Eq. (73). Therefore, we can use a simple interpolation method for velocity in order to obtain efficient ray tracing. One possibility is a velocity distribution defined by linear functions in a sequence of triangles. Given the velocity value at each apex, a linear velocity function is uniquely determined in each triangle. In general, the velocity is continuous across the edges of the triangles but the velocity gradient is discontinuous. The advantage of a linear velocity function is that the ray path is a circle. The method has been used by others (Will, 1976; Whittal and Clowes, 1979; Marks and Hron, 1980).

For simplicity we will only discuss a 2-dimensional model. In 3-dimensions the velocity can be defined by linear functions in a sequence of tetrahedra. Again, the velocity values at the four apexes uniquely define a linear function. In each tetrahedron, the ray is restricted to a plane and the solution is similar to the 2-dimensional triangle. However, the geometry of the surfaces between tetrahedra is considerably more complicated and the ray plane may intersect the tetrahedron in a three- or four-sided figure. We will not discuss these complications here.

In each triangle, the linear velocity function can be completely general. Nevertheless, we can always define a local 'vertical' such that the velocity is a function of only one coordinate. We define a unit vector, $\hat{\mathbf{j}}$, perpendicular to the plane of the ray (fixed) and then define a RH set of axes by local vertical and horizontal vectors, $\hat{\mathbf{k}}$ and $\hat{\mathbf{i}}$,

$$\hat{\mathbf{k}} = -\nabla v/|\nabla v|, \quad \hat{\mathbf{i}} = \hat{\mathbf{j}} \times \hat{\mathbf{k}}. \tag{80}$$

Along the ray, we define another set of RH axes,

$$\hat{\mathbf{n}} = v\mathbf{p}, \quad \hat{\mathbf{m}} = \hat{\mathbf{j}} \times \hat{\mathbf{n}}. \tag{81}$$

These vectors are illustrated in Fig. 16.

In each triangle, the local 'horizontal' slowness (or ray parameter) is conserved as the velocity function is 1-dimensional. To distinguish this from the true horizontal slowness, p, and to indicate the triangle sequence, we use a subscript $_s$. Thus

$$p_s = \mathbf{p} \cdot \hat{\mathbf{i}}_s \tag{82}$$

is the ray parameter in the s-th triangle. The ray path is a circle with radius

$$R_s = 1/p_s|\nabla v_s| \tag{83}$$

and the centre lies at the intersection of the vectors $\hat{\mathbf{m}}_s$ and the line $v_s(z) = 0$. The intersection of a circle with a line reduces to a quadratic equation so it is straightforward to solve for the exit point of the ray. The vectors $\hat{\mathbf{m}}$ and $\hat{\mathbf{n}}$ vary along the ray. We are really only interested in their values at the entry and exit points, indicated with and without a superscript dagger ($^+$), e.g. $\hat{\mathbf{m}}_s^+$ and $\hat{\mathbf{m}}_s$.

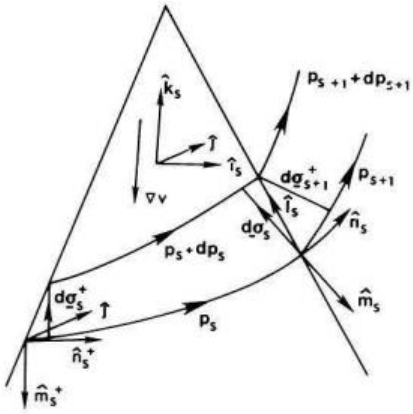

Fig. 16. Neighbouring rays in the s-th triangle and across the s-th interface

The travel time in a linear velocity function is well known (Gebrande, 1976):

$$T_s = [\tanh^{-1}(\hat{\mathbf{n}}_s \cdot \hat{\mathbf{k}}_s) - \tanh^{-1}(\hat{\mathbf{n}}_s^+ \cdot \hat{\mathbf{k}}_s)]/|\nabla v_s|. \tag{84}$$

Note that if a turning point occurs in the triangle, both terms are positive.

In order to calculate the partial derivatives required for the Jacobian (17), it is necessary to consider neighbouring rays through the triangles and across the edges (Fig. 16). We define the cross-section of the ray tube

$$d\boldsymbol{\sigma} = d\sigma\, \hat{\mathbf{m}} \tag{85}$$

and by resolving the cross-section in the local horizontal direction we obtain

$$d\sigma_s(\hat{\mathbf{m}}_s \cdot \hat{\mathbf{i}}_s)^{-1} = d\sigma_s^+(\hat{\mathbf{m}}_s^+ \cdot \hat{\mathbf{i}}_s)^{-1} + dp_s(\partial_{p_s} x_s). \tag{86}$$

The horizontal range and its derivative are

$$x_s = \frac{1}{|\nabla v_s|}\left(\frac{\hat{\mathbf{n}}_s \cdot \hat{\mathbf{k}}_s}{\hat{\mathbf{n}}_s \cdot \hat{\mathbf{i}}_s} v_s - \frac{\hat{\mathbf{n}}_s^+ \cdot \hat{\mathbf{k}}_s}{\hat{\mathbf{n}}_s^+ \cdot \hat{\mathbf{i}}_s} v_s^+\right) \tag{87}$$

$$\partial_{p_s} x_s = \frac{1}{|\nabla v_s|}\left[-\frac{v_s^2}{(\hat{\mathbf{n}}_s \cdot \hat{\mathbf{i}}_s)^2(\hat{\mathbf{n}}_s \cdot \hat{\mathbf{k}}_s)} + \frac{v_s^{+2}}{(\hat{\mathbf{n}}_s^+ \cdot \hat{\mathbf{i}}_s)^2(\hat{\mathbf{n}}_s^+ \cdot \hat{\mathbf{k}}_s)}\right]. \tag{87}$$

On the s-th boundary at the exit of the s-th triangle we need formulae to connect $d\sigma_s$ and $d\sigma_{s+1}^+$, and p_s and p_{s+1} (Fig. 16). We define a unit vector along the boundary $\hat{\mathbf{l}}_s$ (sign arbitrary). In the figure we have illustrated a transmission, but the same notation can be used for reflections. The subscript $_s$ enumerates triangles and boundaries along a ray, not specific triangles.

The rays are connected across the boundary using Snell's law:

$$\frac{\hat{\mathbf{n}}_s \cdot \hat{\mathbf{l}}_s}{v_s} = \frac{\hat{\mathbf{n}}_{s+1}^+ \cdot \hat{\mathbf{l}}_s}{v_{s+1}^+}. \tag{88}$$

The cross-sections can be connected via the boundary element:

$$d\hat{\mathbf{l}}_s = \frac{d\sigma_s}{\hat{\mathbf{l}}_s \cdot \hat{\mathbf{m}}_s}\hat{\mathbf{l}}_s = \frac{d\sigma^+_{s+1}}{\hat{\mathbf{l}}_s \cdot \hat{\mathbf{m}}^+_{s+1}}\hat{\mathbf{l}}_s. \tag{89}$$

The formula to connect dp_s and dp_{s+1} is somewhat more complicated. From the definition of the ray parameter we have

$$dp_s = \frac{d\hat{\mathbf{n}}_s \cdot \hat{\mathbf{l}}_s}{v_s} - \frac{(\hat{\mathbf{n}}_s \cdot \hat{\mathbf{l}}_s)\, dv_s}{v_s^2} \tag{90}$$

and similarly for dp_{s+1}. From Snell's law, Eq. (88), we obtain

$$\frac{d\hat{\mathbf{n}}_s \cdot \hat{\mathbf{l}}_s}{v_s} - \frac{(\hat{\mathbf{n}}_s \cdot \hat{\mathbf{l}}_s)\, dv_s}{v_s^2} = \frac{d\hat{\mathbf{n}}^+_{s+1} \cdot \hat{\mathbf{l}}_s}{v^+_{s+1}} - \frac{(\hat{\mathbf{n}}^+_{s+1} \cdot \hat{\mathbf{l}}_s)\, dv^+_{s+1}}{v^{+2}_{s+1}}. \tag{91}$$

These expressions can be simplified using

$$d\hat{\mathbf{n}} = dn\,\hat{\mathbf{m}} \tag{92}$$

and the velocity differential eliminated using

$$dv_s = \nabla v_s \cdot d\hat{\mathbf{l}}_s = -\frac{\hat{\mathbf{l}}_s \cdot \hat{\mathbf{k}}_s}{\hat{\mathbf{l}}_s \cdot \hat{\mathbf{m}}_s}\,|\nabla v_s|\, d\sigma_s \tag{93}$$

and similarly for dv^+_{s+1}. The final expression connecting dp_s and $d\sigma_s$ with dp_{s+1} and $d\sigma^+_{s+1}$ can be written

$$\boldsymbol{\sigma}^+_{s+1} = \mathbf{R}_s \mathbf{S}_s \mathbf{Q}_s \boldsymbol{\sigma}_s \tag{94}$$

where we have defined a vector $\boldsymbol{\sigma} = (d\sigma, dp)^T$. The 2×2 matrices are

$$\begin{aligned}
&R_{11} = 1, \quad R_{12} = 0, \quad R_{21} = -\frac{(\hat{\mathbf{l}}_s \cdot \hat{\mathbf{k}}_{s+1})^2\, |\nabla v_{s+1}|}{(\hat{\mathbf{l}}_s \cdot \hat{\mathbf{m}}^+_{s+1})^2\, v^{+2}_{s+1}},\\
&R_{22} = \frac{\hat{\mathbf{l}}_{s+1} \cdot \hat{\mathbf{m}}^+_{s+1}}{\hat{\mathbf{l}}_s \cdot \hat{\mathbf{m}}^+_{s+1}};\\
&S_{11} = \frac{\hat{\mathbf{l}}_s \cdot \hat{\mathbf{m}}^+_{s+1}}{\hat{\mathbf{l}}_s \cdot \hat{\mathbf{m}}_s}, \quad S_{12} = S_{21} = 0, \quad S_{22} = 1;\\
&Q_{11} = 1, \quad Q_{12} = 0, \quad Q_{21} = \frac{(\hat{\mathbf{l}}_s \cdot \hat{\mathbf{k}}_s)^2\, |\nabla v_s|}{(\hat{\mathbf{l}}_s \cdot \hat{\mathbf{m}}_s)(\hat{\mathbf{l}}_s \cdot \hat{\mathbf{m}}_s)\, v_s^2},\\
&Q_{22} = \frac{\hat{\mathbf{l}}_s \cdot \hat{\mathbf{m}}_s}{\hat{\mathbf{l}}_s \cdot \hat{\mathbf{m}}_s}.
\end{aligned} \tag{95}$$

This separation is convenient as $\mathbf{Q}_s$ is calculated in the s-th triangle, $\mathbf{S}_s$ at the s-th interface, and $\mathbf{R}_s$ in the $(s+1)$-th triangle. We write the propagation across the s-th triangle as

$$\boldsymbol{\sigma}_s = \mathbf{T}_s \boldsymbol{\sigma}^+_s \tag{96}$$

where

$$T_{11} = \frac{\hat{\mathbf{m}}_s \cdot \hat{\mathbf{l}}_s}{\hat{\mathbf{m}}^+_s \cdot \hat{\mathbf{l}}_s}, \quad T_{12} = \frac{T_{11} - 1}{p_s^2\, |\nabla v_s|}, \quad T_{21} = 0, \quad T_{22} = 1. \tag{97}$$

Thus the complete transmission through a sequence of triangles can be written

$$\boldsymbol{\sigma}_n = \mathbf{T}_n \mathbf{R}_{n-1} \mathbf{S}_{n-1} \mathbf{Q}_{n-1} \ldots \mathbf{R}_1 \mathbf{S}_1 \mathbf{Q}_1 \mathbf{T}_1 \boldsymbol{\sigma}^+_1. \tag{98}$$

This system of equations can be used to find the derivatives required for the Jacobians.

Conclusions

The generalization of ART described in this paper, particularly the result (45), has solved simply some of the canonical problems. The result is not significantly more complicated to compute than normal ART as the same kinematic, Eq. (13), and dynamic, Eq. (20), ray tracing is required. In fact, because two-point ray tracing is not needed and small, numerical features are automatically smoothed out, Eq. (73), the result is easier to compute than normal ART.

Expression (45) is valid for direct and normal turning rays with any number of turning points, reversed turning rays with any number of turning points, partial and total reflections, and transmissions. For these signals, the result (45) reduces to normal ART [Eq. (5) with $n=0$] if the amplitude function, $\tilde{A}^{(0)}(\mathbf{y})$, is constant and the phase function, $\tilde{\theta}(p, \mathbf{x})$, parabolic. In as much as expression (45) includes variations from this, it is more accurate. It also remains valid at critical points, Airy caustics and Fresnel shadows. In laterally homogeneous media, it describes head waves and Fresnel diffractions accurately. They are generated by discontinuities in the amplitude function at critical and end points, respectively. In laterally inhomogeneous media these signals are described incorrectly both in time and amplitude. 'Head wave' arrivals are obtained with constant slowness as if the interface were plane through the critical point. Fresnel diffractions extrapolate the discontinuous wavefront with constant slowness without regard to the inhomogeneous structure through which the wave propagates. It remains an unsolved problem to model these signals in a general, straightforward fashion.

It was not expected that the other canonical problems could be solved by a simple extension of ART. In the case of interference head waves, edge, point and interface diffractions the boundary conditions are obviously vital (and complicated). For gradient coupling, it is known from 1-dimensional experience that an iterative rather than asymptotic solution is needed. Although canonical problems can be solved, and combined with ART, they are sufficiently complicated, particularly for elastodynamics, that they have not been widely used. Seismic modelling has progressed sufficiently that this situation must now be rectified.

References

Arnol'd, V.I.: Characteristic classes entering in quantization conditions. Funct. Anal. Appl. **1**, 1–13, 1967

Burridge, R.: The reflexion of a pulse in a solid space. Proc. Roy. Soc. A **276**, 367–400, 1963a

Burridge, R.: The reflexion of a disturbance within an elastic sphere. Ph. D. thesis, University of Cambridge, 1963b

Cagniard, L.: Réflexion et réfraction des ondes séismiques progressives. Paris: Gauthier-Villars 1939

Cagniard, L.: Reflexion and refraction of progressive seismic waves, trans. E.A. Flinn and C.H. Dix. New York: McGraw-Hill Book Co. 1962

Červený, V., Ravindra, R.: Theory of seismic head waves. Toronto: University of Toronto Press 1971
Červený, V., Molotkov, I.A., Pšenčík, I.: Ray method in seismology. Prague: Charles University Press 1977
Chapman, C.H.: A new method for computing synthetic seismograms. Geophys. J.R. Astron. Soc. **54**, 481–518, 1978
Chapman, C.H.: Long-period corrections to body-waves: theory. Geophys. J.R. Astron. Soc. **64**, 321–372, 1981
Chapman, C.H., Drummond, R.: Body-wave seismograms in inhomogeneous media using Maslov asymptotic theory. Bull. Seismol. Soc. Amer. **72**, S277–S317, 1982
Courant, R., Hilbert, D.: Methods of mathematical physics. New York: John Wiley and Sons 1962
Gebrande, H.: A seismic-ray tracing method for two-dimensional inhomogeneous media. In: Exploration seismology in Central Europe: data and results, P. Giese, C. Prodehl and A. Stein, eds., pp 162–167. Berlin: Springer 1976
Gilbert, F.: Scattering of impulsive elastic waves by a smooth convex cylinder. J. Acous. Soc. Amer. **32**, 841–856, 1960
Gilbert, F., Backus, G.E.: Propagator matrices in elastic wave and vibration problems. Geophysics **31**, 326–333, 1966
Heyman, E., Felsen, L.B.: Non-dispersive approximations for transient ray fields in an inhomogeneous medium. In: Proceedings of the NATO Advanced Research Workshop on Hybrid Formulation of Wave Propagation and Scattering. Nijhoff Publishing Co. 1984
Hill, D.P.: Critical refracted waves in a spherically symmetric, radially heterogeneous Earth model. Geophys. J.R. Astron. Soc. **34**, 149–179, 1973
de Hoop, A.T.: A modification of Cagniard's method for solving seimic pulse problems. Appl. Scient. Res. B **8**, 349–356, 1960
Hörmander, L.: Fourier integral operators. Acta Math. **127**, 79–183, 1971
Hörmander, L.: Spectral analysis of singularities. In: Seminar on singularities of solutions of linear partial differential equations, L. Hörmander, ed.: pp 3–49. Princeton: Princeton Univ. Press 1979
Hron, F., Kanasewich, E.R.: Synthetic seismograms for deep seismic sounding studies using asymptotic ray theory. Bull. Seismol. Soc. Amer. **61**, 1169–1200, 1971
Jackson, P.S.: The focusing of earthquakes. Bull. Seismol. Soc. Amer. **61**, 685–695, 1971
Keller, J.B.: Corrected Bohr-Sommerfeld quantum conditions for non-separable systems. Ann. Phys. **4**, 180–188, 1958
Keller, J.B.: The geometrical theory of diffraction. J. Opt. Soc. Amer. **52**, 116–130, 1962
Kennett, B.L.N., Illingworth, M.R.: Seismic waves in a stratified half space – III. Piecewise smooth models. Geophys. J.R. Astron. Soc. **66**, 633–675, 1981
Kline, M., Kay, I.W.: Electromagnetic theory and geometrical optics. New York: John Wiley and Sons 1965
Knopoff, L., Gilbert, F.: Diffraction of elastic waves by the core of the earth. Bull. Seismol. Soc. Amer. **51**, 35–49, 1961
Ludwig, D.: Uniform asymptotic expansion at a caustic. Comm. Pure Appl. Math. **29**, 215–250, 1966
McMechan, G.A., Mooney, W.D.: Asymptotic ray theory and synthetic seismograms for laterally varying structures: theory and application to the Imperial Valley, California. Bull. Seismol. Soc. Amer. **70**, 2021–2035, 1980
Madariaga, R.: Gaussian beam synthetic seismograms in a vertically varying medium. Geophys. J.R. Astron. Soc. **79**, 589–612, 1984
Marks, L.W., Hron, F.: Weber function computation in the interference reflected head wave amplitude. Geophys. Res. Lett. **4**, 255–258, 1977
Marks, L.W., Hron, F.: Calculation of synthetic seismograms in laterally inhomogeneous media. Geophysics **45**, 509–510, 1980
Maslov, V.P.: Theory of perturbations and asymptotic methods (in Russian). Moscow: Izd. MGU 1965
Milnor, J.: Morse theory. Princeton: Princeton Univ. Press 1969
Pekeris, C.L.: The seismic surface pulse. Proc. Nat. Acad. Sci. USA **41**, 469–480, 1955a
Pekeris, C.L.: The seismic buried pulse. Proc. Nat. Acad. Sci. USA **41**, 629–639, 1955b
Richards, P.G., Frasier, C.W.: Scattering of elastic waves from depth-dependent inhomogeneities. Geophysics **41**, 441–458, 1976
Scholte, J.G.J.: Oblique propagation of waves in inhomogeneous media. Geophys. J.R. Astron. Soc. **7**, 244–261, 1962
Smirnov, V.I.: A course in higher mathematics, Vol. 4, trans. D.E. Brown and I.N. Sneddon. Oxford: Pergammon Press 1964
Stickler, D.C., Ahluwalia, D.S., Ting, L.: Application of Ludwig's uniform progressing wave ansatz to a smooth caustic. J. Acous. Soc. Amer. **69**, 1673–1681, 1981
Thomson, C.J., Chapman, C.H.: An introduction to Maslov's asymptotic method. Geophys. J.R. Astron. Soc. 1985 (in press)
Whittal, K.P., Clowes, R.M.: A simple, efficient method for the calculation of travel-times and ray paths in laterally inhomogeneous media. J. Can. Soc. Exp. Geophys. **15**, 21–29, 1979
Will, M.: Calculation of travel-times and ray paths for lateral inhomogeneous media. In: Explosion seismology in Central Europe: dates and results, P. Giese, C. Prodehl and A. Stein, eds.: pp 168–177. Berlin: Springer-Verlag 1976
Ziolkowski, R.W., Deschamps, G.A.: Asymptotic evaluation of high frequency fields near a caustic: an introduction to Maslov's method. Radio Science **19**, 1001–1025, 1984

Received February 5, 1985; revised version May 7, 1985
Accepted May 8, 1985
Department of Earth Sciences publication No. 612